



SEISMIC OBSERVATIONS OF METEORS: COUPLING THEORY AND OBSERVATIONS

Wayne N. Edwards,¹ David W. Eaton,^{1,2} and Peter G. Brown³

Received 24 October 2007; accepted 16 June 2008; published 31 December 2008.

[1] Over the last century, seismic instruments have recorded, with increasing frequency, the ground motion produced by meteorically generated shock waves striking the Earth's surface. In this review, the history of meteor-related seismic signals is discussed, along with documented waveform characteristics, source mechanisms, air-ground coupling phenomena, and kinematic methods of determining meteor trajectories and event locations. Uncertainties in the mechanics of air-ground coupling, however, have left methods of measuring meteor source energy underdeveloped.

Citation: Edwards, W. N., D. W. Eaton, and P. G. Brown (2008), Seismic observations of meteors: Coupling theory and observations, *Rev. Geophys.*, 46, RG4007, doi:10.1029/2007RG000253.

1. INTRODUCTION

[2] Although seismology and seismic instruments are primarily focused upon studying the structure, properties, and motions of Earth's interior, they can also be useful tools for studying the dynamics of objects that produce infrasonic airwaves during their flight through the atmosphere. Among these are airwaves associated with supersonic jets [e.g., *McDonald and Goforth*, 1969; *Kanamori et al.*, 1992; *Cates and Sturtevant*, 2002], explosions, lightning [*Lin and Langston*, 2007], volcanic activity [e.g., *Garcés and Hansen*, 1998; *Ripepe et al.*, 2001], and missile and other military munitions firings [e.g., *Cochran and Shearer*, 2006]. Another phenomenon which produces distinct atmospheric infrasonic signals that may produce seismic waves is meteoroids as they interact with Earth's atmosphere. Indeed, with recent global proliferation of seismograph stations and networks, the number of recorded meteor-related seismic observations is also increasing rapidly. A summary of published meteor seismic events is given in Tables 1a and 1b. Such ground-coupled acoustic waves have been used to reconstruct meteoroid trajectories, to constrain meteoroid

To date, coupling of acoustic waves directly with the Earth's surface represents the bulk of the observed meteor-related seismic signals, while precursory and impact-related seismic waves remain an observational rarity. With proliferation of infrasound and seismic monitoring systems, new opportunities exist to explore the relationship between Earth's atmosphere and surface. Continued study of meteor seismology will lead to new methods to constrain energies, sizes, and fluxes for moderately (cm to m) sized meteoroids on Earth and potentially on Mars.

events in position and time, to obtain source body kinetic energy estimates, and to facilitate the search for meteorites on the ground. The growing number of seismograph stations and areas being monitored thus provides an increasingly powerful instrumental means for remote detection and characterization of meteors on a global scale. With such a capability, future plans for seismograph deployments on Mars hold the promise that seismic meteoroid detection techniques could provide the first detailed flux estimates for meter-sized impactors at the Martian surface, a topic of considerable recent interest [*Malin et al.*, 2006].

[3] Air-coupled seismic waves produced by meteors have been recorded as early as 1908, after the Great Siberian Meteor exploded over the Tunguska River on 30 June 1908 [*Whipple*, 1930; *Ben-Menahem*, 1975]. The Tunguska event is often cited as the classic example of meteor-generated infrasound, yet it also represents the earliest and most energetic example of a seismic recording of a meteor. Infrasound-coupled waves from the explosion, as well as independently propagating surface waves, were recorded at four Russian stations between 973 and 5293 km from the event [*Ben-Menahem*, 1975]. The explosion also produced gravity waves and led to large-scale oscillations of Earth's atmosphere [*Whipple*, 1934]. In terms of energy, Tunguska was the largest meteor explosion ever recorded, with estimates of the meteor energy equivalent to a 12.5 Mt explosion [*Ben-Menahem*, 1975]. In contrast, most modern observations are made in much closer proximity to the

¹Department of Earth Sciences, University of Western Ontario, London, Ontario, Canada.

²Now at Department of Geoscience, University of Calgary, Calgary, Alberta, Canada.

³Department of Physics and Astronomy, University of Western Ontario, London, Ontario, Canada.

TABLE 1A. Modern and Historical Seismic Detections of Meteoroids

Date	Event	Latitude	Longitude	Country	Observations	Seismic Interpretation	References
30 Jun 1908	Great Siberian Meteor	60.917°N	101.950°E	Russia	4	seismic body waves	<i>Ben-Menahem</i> [1975]
31 Mar 1965	Revelstoke meteorite fall	51.6°N	118.6°W	Canada	4	acoustic: point	<i>Folinsbee et al.</i> [1967]
6 Feb 1967	Vilna meteorite fall	54.23°N	111.69°W	Canada	1	acoustic: point?	<i>Folinsbee et al.</i> [1969]
20 Aug 1969	Prince George fireball	53.83°N	122.44°W	Canada	3	meteorite impact?	<i>Halliday and Blackwell</i> [1971]
8 Mar 1975	Kirin meteorite fall			Jilin Province, China	2	meteorite impact	<i>Joint Investigation Group on the Kirin Meteorite Shower</i> [1977]
10 May 1977	Plains of Kanto fireball	36.966°N	140.295°E	Japan	4	acoustic: shock wave	<i>Nagasawa</i> [1978]
1 Jun 1982	Cold Lake meteor	54.2928°N	112.8011°W	Canada	9	acoustic: shock wave	<i>Cumming</i> [1989]
19 Sep 1986	Yellowknife meteor	62.5°N	114.6°W	Canada	17	acoustic and Rayleigh waves	<i>Anglin and Haddon</i> [1987, 1988]
11 Sep 1987	Chugoku fireball	34.28°N	133°E	Japan	8	acoustic: shock wave	<i>Nagasawa and Miura</i> [1987]
20 Jan 1988	Strathcona Park fireball	49.495°N	125.543°W	Canada	1	acoustic: point	<i>Aikman et al.</i> [1989]
25 Jan 1989	Mount Adams fireball	46.396°N	122.062°W	USA	26	acoustic: point (× 2)	<i>Qamar</i> [1995]
20 Jan 1988	Lugo fireball	44.48°N	11.91°E	Italy	5	acoustic: point	<i>Cevolani et al.</i> [1993, 1994] and <i>Foschini</i> [1998]
15 Jun 1994	St.-Robert meteorite fall	45.9°N	73.0°W	Canada	1 (?)	acoustic	<i>Brown et al.</i> [1996] and <i>Hildebrand et al.</i> [1997]
9 Oct 1996	El Paso bolide	31.80°N	106.06°W	USA	5	acoustic: point	<i>Hildebrand et al.</i> [1999] and <i>Edwards and Hildebrand</i> [2004]
30 Mar 1998	Miyako fireball	39°N	142°E	Japan	26	acoustic: shock wave	<i>Ishihara et al.</i> [2003a]
26 Sep 1999	Kobe meteorite fall	35°N	135°E	Japan	56	acoustic: shock wave	<i>Ishihara et al.</i> [2003b]
18 Jan 2000	Tagish Lake meteorite fall	59.7°N	134.2°W	Canada	2	acoustic: shock wave	<i>Brown et al.</i> [2002b]
6 May 2000	Morávka meteorite fall	49.90°N	18.48°E	Czech Republic	16	acoustic: point (multiple)	<i>Brown et al.</i> [2003] and <i>Borovička and Kalenda</i> [2003]
9 Dec 2000	Tahiti fireball	17.9°S	149.5°W	Tahiti	8	acoustic: shock wave	<i>Le Pichon et al.</i> [2002]
4 Nov 2003	Arkansas bolide	36°N	90°W	USA	22	acoustic: shock wave	<i>Langston</i> [2004]
27 Mar 2003	Park Forest meteorite fall	41.46°N	87.73°W	USA	1	acoustic: point	<i>Brown et al.</i> [2004]
6 Apr 2003	Neuschwanstein meteorite fall	10.8507°N	47.5257°E	Austria/Germany	9	acoustic: shock wave	<i>ReVelle et al.</i> [2004]
16 Jun 2003	Kanto fireball	36.5°N	140°E	Japan	40	acoustic: shock wave	<i>Ishihara et al.</i> [2004]
3 Jun 2004	Washington State bolide	47.96°N	121.976°W	USA	99	acoustic: point	<i>Arrowsmith et al.</i> [2007]
24 Jan 2004	Villalbeto de la Peña meteorite fall	42.843°N	4.711°W	Spain	1	acoustic: point	<i>Llorca et al.</i> [2005]
11 Dec 2004	Lanzhou bolide	36.052°N	104.454°E	China	8	acoustic: shockwave and point	<i>Daiju and Yarong</i> [2007]
10 Sep 2005	Ischia bolide	40.6°N	13.8°E	Italy	21	acoustic: shockwave and point	<i>D'Auria et al.</i> [2006]

TABLE 1B. Seismic Detections of Man-Made Atmospheric Events

Date	Detected Object	Latitude	Longitude	Country	Observations	Seismic Interpretation	References
1963	supersonic aircraft			California/Arizona/Utah, USA		acoustic: shock wave	<i>McDonald and Goforth</i> [1969]
19 Sep 1980	missile silo explosion			Kentucky/Tennessee, USA		acoustic: point	<i>Johnston</i> [1987]
and 12 Oct 1982	and supersonic aircraft						
1989/1991	space shuttle reentries			Southern California, USA	39	acoustic: shock wave	<i>Kanamori et al.</i> [1991, 1992]
8 Dec 1993 and	supersonic aircraft			Southern California, USA	64+	acoustic: shock wave	<i>Cates and Sturtevant</i> [2002]
30 Jan 1992	and space shuttle <i>Discovery</i>						
15 Jan 2006	NASA Stardust reentry	40.41°N	113.87°W	USA	2	acoustic: shock wave	<i>ReVelle and Edwards</i> [2007] and <i>Edwards et al.</i> [2007]

meteoroid’s trajectory, typically at ranges up to a few 100 km. Similarly, source energies rarely exceed a few kilotons of TNT ($1 \text{ kt} = 4.185 \times 10^{12} \text{ J}$) as expected because of the much higher flux of objects of smaller sizes at the Earth [Brown et al., 2002a].

[4] In order to understand the dynamics of airwave coupling to ground motion, it is necessary to reconcile incompatible theoretical treatments of Earth’s surface that arise in the disciplines of atmospheric infrasound and seismology. From an atmospheric infrasound perspective, Earth’s surface is conveniently regarded as a rigid half-space, whereas from a seismological perspective the ground is typically viewed as a free surface at which stresses vanish. More complete treatments of Earth’s surface as a fluid-solid contact, or a contact between a fluid and a porous soil layer, yield expressions that relate atmospheric overpressure to ground motion. Similarly, more complete models of the atmosphere and Earth such as layered structure in the near surface give rise to further complexities, such as coupled interface modes.

[5] The objectives of this review are to compile observations of seismic detection of meteoroids, synthesizing results from the disciplines of seismology and atmospheric infrasound in order to characterize the associated physical processes. Three distinct mechanisms of air-ground coupling exist; these mechanisms are each considered in turn, with reference to published observations, underlying physical principles, and areas where uncertainties remain. This review also highlights the physical characteristics of meteoroid entry that may be inferred from seismic observations, the limitations to our interpretations due to the complex nature of meteoroid ablation (i.e., fragmentation effects), along with future prospects for new insights into meteoroid structure, mass, and energy that may be determined using seismic observations.

2. PHYSICAL PROCESSES OF AIRWAVE GENERATION AND GROUND COUPLING

[6] The physics of airwave production and subsequent ground coupling is relatively straightforward in principle, although some details remain uncertain. When a meteoroid encounters Earth’s atmosphere at hypersonic velocity, a ballistic shock wave is produced within a narrow Mach cone of half angle β , with the meteoroid located at its apex (Figure 1). The extreme velocities of these objects (ranging between approximately Mach 35 and Mach 240) result in a sufficiently small Mach cone angle such that the wavefront of this cone may be approximated as cylindrical [ReVelle, 1974, 1976]. Within a few dozen to hundreds of meters perpendicular to the trajectory, depending on source energy [ReVelle, 1976], the hypersonic shock wave slows to acoustic wave speeds (varying between ~ 280 and 340 m/s between 100 km altitude and the surface) as it propagates outward from the source.

[7] In some cases, additional shock waves with quasi-spherical wavefronts are produced by meteoroid fragmentation. For this class of meteors, often referred to as bolides,

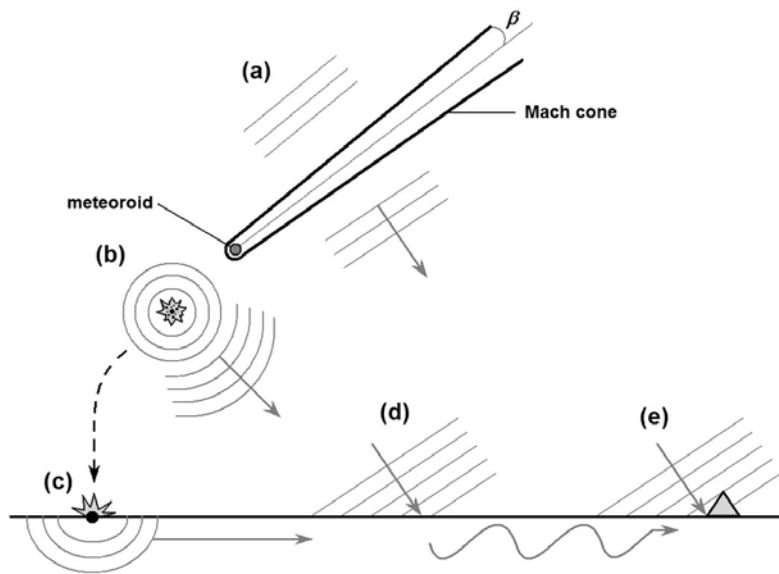


Figure 1. Schematic diagram of meteor-generated atmospheric waves and mechanisms of airwave seismic generation. (a) Generation of shock waves during hypersonic entry. Propagation is preferentially perpendicular to meteor’s trajectory. (b) Generation of shock wave during meteoroid fragmentation. Propagation is omnidirectional or quasi-point-like. (c) Seismic wave generation during meteorite impacts. (d) Seismic precursor wave generation through matching of surface wave speeds (P , S , or Rayleigh). Travel via surface speeds allows these waves to arrive prior to (e) direct coupling of the atmospheric pressure wave with the surface at the site of the seismic station (gray triangle).

the structural strength of the meteoroid is less than the air ram pressure. When this condition is reached, the meteoroid undergoes sudden and violent fragmentation that may obliterate the object entirely into fine particles [e.g., Klekociuk *et al.*, 2005] or cause it to fragment into a number of smaller pieces, each of which may then continue to ablate and/or fall to the surface as meteorites. The airwave produced in this case is often referred to as an ablational shock [Bronsthen, 1983].

[8] Acoustic waves experience frequency-dependent attenuation as they propagate in the atmosphere. In general, only acoustic waves in the infrasonic band ($\sim 0.001\text{--}20$ Hz) impinge upon Earth’s surface with sufficient energy to induce measurable ground motion. As first noted by Cumming [1989], there are three basic mechanisms by which such infrasonic waves may couple into the subsurface (direct, precursory, and impact):

[9] 1. Direct coupling is the mechanism whereby seismic waves result from the local loading of the surface by the overpressure of an incident acoustic wave.

[10] 2. Precursory arrivals are a result of the generation of surface and/or head waves by incident acoustic waves at specific incidence angles with respect to the ground. These waves then propagate to the observing station independently from the incident acoustic wave. Such waves generally precede direct arrivals.

[11] 3. Impact coupling is the generation of surface and/or body waves by the impact of a meteorite(s) onto Earth’s surface.

[12] These three mechanisms are not equally common. Direct coupling is observed most commonly, followed by precursory coupling (rare) and impact coupling (extremely rare, not one well-documented case to date). In sections 3–6, theory and observational constraints pertinent to each of these three different mechanisms are described and discussed.

3. SEISMIC DETECTION OF METEORITE IMPACT

[13] Impacts on Earth are much more difficult to detect than is the case for an airless and seismically quiet body such as the Moon. Lunar seismic detections of meteoroid impacts were common during the operational lifetime of the Apollo seismic network [Dorman *et al.*, 1978; Oberst and Nakamura, 1991]. On Earth, the vast majority of meteoroids are reduced by ablation to kilogram-sized or smaller fragments and slowed by atmospheric drag to a terminal velocity of only a few hundred m/s. The kinetic energy of such small impactors (meteorites) is insufficient to produce ground motion that is observable beyond a few km from the source [e.g., Johnston, 1987]. Only very large (and extremely rare) meteorite impacts retain a sufficient fraction of their original velocity to reach the Earth with enough energy to produce explosive-type craters [Bland and Artemieva, 2006]. Excluding the improbable scenario of impact occurring very close to a seismograph station, direct seismic detection of meteorite impact is effectively limited to objects greater than ~ 50 kg [Nicholls and Stewart, 1974].

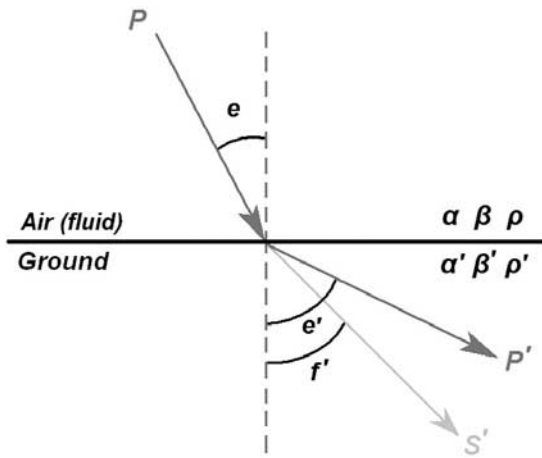


Figure 2. Geometry of a fluid (atmosphere) and solid (surface) boundary in welded contact, as discussed by *Ben-Menahem and Singh* [1981, 2000].

[14] Because of the rarity of such large meteorite impacts, seismic observations of events are exceedingly rare. Only once, after a suspected meteorite fall near Prince George, British Columbia, Canada, has there been a published interpretation, supported by data, of seismic waves caused by a meteorite impact [*Halliday and Blackwell*, 1971]. On the basis of interpretation of the seismic signals, Halliday and Blackwell inferred it to be composed of iron, weighing no less than 1.2×10^4 kg. As no meteorite from this fall was ever recovered, nor any sign of a crater or plunge pit identified, the interpretation of the source of the seismic arrivals from this event must be regarded as provisional. Inspection of the original records by the present authors suggests that the seismic waves were locally coupled air seismic waves (precursor waves, see section 4), perhaps enhanced because of topographic coupling, rather than impact induced. The only other case, to our knowledge, is a report on the Kirin meteorite fall on 8 March 1976 in the Kirin province of China, where a meteorite (ordinary H chondrite) weighing 1770 kg created an ~ 2 m wide plunge pit and came to rest ~ 6 m below the surface [*Joint Investigation Group on the Kirin Meteorite Shower*, 1977]. Among the various aspects of the fall reported is the mention of the seismic recording of the impact by two stations (Fengman at 2302:46 UT and Kirin at 2302:50 UT) that allowed the time of impact to be estimated at 2302:36 UT. Unfortunately, the seismic waveform observations were not included in the report, making verification of the interpretation difficult. Regardless, this remains the only case in which such a seismic recording has been reported with links to a documented meteorite impact.

[15] Nevertheless, seismic waves from modest impactors (\sim tonne masses) should be detectable. Though meteorite falls of such large masses producing simple impact craters on the Earth are rare, iron impactors, in particular, are often able to reach the ground relatively intact at supersonic velocities [cf. *Bland and Artemieva*, 2006]. In such instan-

ces, craters of order ~ 10 – 20 m in diameter may be produced [*Collins et al.*, 2005]. The seismic signature for such an event depends critically on the seismic coupling efficiency of the impact, a value which is poorly known. *Shishkin* [2007] has developed a simple theory for this coupling and finds that for small impacts an efficiency 1–10% is most probable; this is similar to the efficiency found for small surface contact explosions reflecting the comparable physics of both processes. This is higher than the often quoted value of 10^{-4} [*Collins et al.*, 2005] which is more appropriate to the lower seismic efficiency of larger (kilometer-scale) impacts. Using this higher efficiency and adapting the Gutenberg-Richter magnitude energy scale from *Collins et al.* [2005] we find that a small impactor (\sim meter sized) having an energy W (in Joules) would produce a seismic magnitude M of

$$M = 0.67 \log_{10} W - 4.53. \quad (1)$$

[16] We remark that there is also a remarkable paucity of hydroacoustic detections of marine impacts. Since oceans cover almost 71% of Earth’s surface area and infrasound waves propagate over large distances with high efficiency and negligible scattering in the marine SOFAR channel waveguide [*Urick*, 1983; *Jensen et al.*, 2000], it seems reasonable to expect that hydroacoustic detection of marine impacts should be more common than seismic detections of impacts on land. Yet, to the authors’ knowledge, there are no published recordings or reports of a marine impact despite more than half a century of global hydroacoustic monitoring. Although the coupling efficiency of impact-generated wave energy into the SOFAR channel is uncertain, we suspect that such events may simply have passed unrecognized; thus, careful reappraisal and continued monitoring of hydroacoustic records may be warranted. Hydroacoustic measurements of any oceanic meteorite impacts (or air-ocean coupling of meteor shocks) could provide valuable estimates of meteoroid terminal mass (total surviving meteoroid mass after atmospheric ablation) for events which otherwise have no means of ground truth in the form of recoverable meteorites.

4. PRECURSORY SEISMIC WAVES

[17] Like impact-generated seismic waves, precursory seismic arrivals are extremely rare. Such waves represent a type of resonant phenomenon that arises from angle-dependent transmissivity of infrasound waves into the subsurface predicted by some theoretical formulations of the air-ground interface (Figure 2). Specifically, the most efficient coupling at a fluid-solid contact occurs when the infrasonic trace velocity (apparent horizontal velocity of the air wave) precisely matches the horizontal velocity of a particular seismic wave mode (Figure 3a), such as the fundamental-mode Rayleigh wave [*Ben-Menahem and Singh*, 1981].

[18] Under such a condition, theoretical models predict the generation of an independently propagating seismic

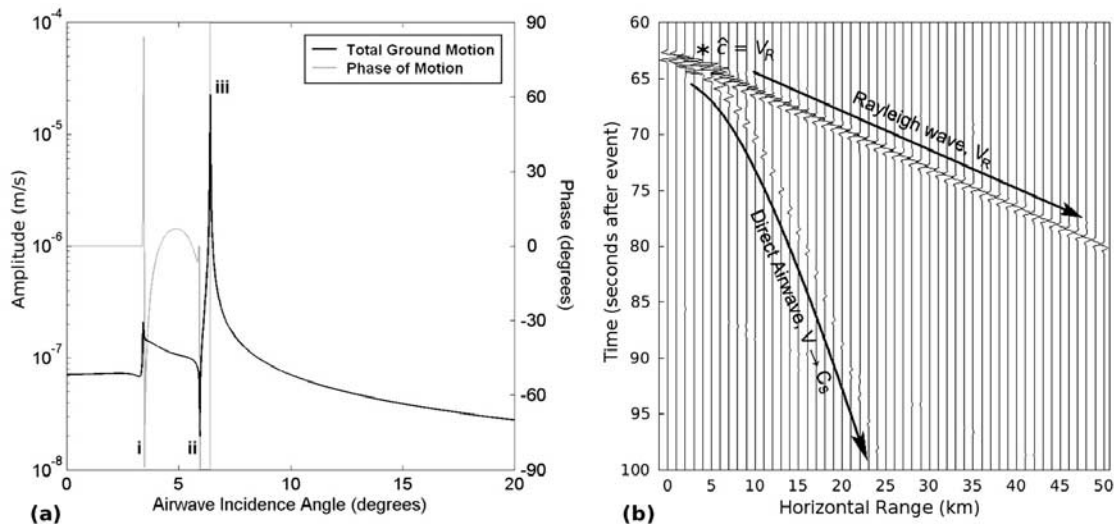


Figure 3. (a) Amplitude and phase of ground motion at a granitic surface ($C_S = 0.320$ km/s, $\rho_{\text{air}} = 1.39$ kg/m³, $V_P = 5.40$ km/s, $V_S = 3.12$ km/s, and $\rho = 2600$ kg/m³) due to a 1 Pa planar atmospheric wave at a fluid-solid interface in welded contact, following the treatment given by *Ben-Menahem and Singh* [1981, 2000]. Note changes in the coupling as the airwave reaches apparent horizontal velocities matching V_P (indicated by i), V_S (indicated by ii), and V_R , the Rayleigh wave velocity (indicated by iii). (b) Synthetic seismogram vertical component traces of a hypothetical airwave (point source at altitude = 20 km) propagating across the same granitic surface. Note the relative amplitudes and time delay between the Rayleigh precursor surface wave and the directly coupled airwave as the horizontal airwave velocity approaches C_S (arrow). Asterisk indicates range where apparent airwave velocity, \hat{c} , equals V_R .

wave, generated within a distributed source region defined by the locus of points where the above excitation condition is met. For example, in the case of a cylindrical air wave produced by a hypersonic object in the atmosphere, this excitation mode would produce outward propagating seismic waves in the surface with mirror symmetry along the projected ground path of the object, whereas for a spherical wavefront produced by a point source such as a fragmentation event, this excitation mode would produce outward propagating waves with cylindrical symmetry from the epicenter of the event.

[19] Since the horizontal trace velocity of the infrasound wave is given by the acoustic velocity divided by the sine of the incidence angle, e (Figure 2), a necessary condition for this phenomenon to occur is that the coupled seismic wave mode must have velocity greater than the acoustic wave speed in air. This is generally the case if bedrock or low-porosity overburden is exposed at the surface. Figures 3 and 4 show a numerical simulation of this phenomenon for the simple case of a lower half-space characterized by average seismic properties of granitic bedrock, representative of a seismograph station located in a shield region. Because of the extreme contrast in seismic properties at the surface interface, synthetic seismograms were computed using a highly numerically stable implementation of the widely used reflectivity algorithm [Wang, 1999]. In this example, the dominant precursory seismic phase predicted by the numerical simulation is a fundamental-mode Rayleigh wave (see section 4.1), but numerical studies indicate that other

types of coupled seismic waves such as P and S head waves may also be generated [Langston, 2004].

[20] These synthetic seismogram calculations show that should multiple stations obtain similar observations of a remotely generated Rayleigh wave, it would appear as if the wave were radiating from either an annular or extended region (Figure 4). However, this mode of coupling remains largely unobserved, with only a single documented case in the literature. This example relates to a meteor that occurred in 1985 near the Yellowknife seismic array, located within the Canadian Shield in the Northwest Territories, Canada [Anglin and Haddon, 1987, 1988]. Although this is the sole well-documented example of this phenomenon, less definitive identifications exist as well (Figure 5). Furthermore, precursory Rayleigh and P/S phases have also been observed in southwest Texas associated with acoustic shocks from space shuttle reentries [Sorrells et al., 2002].

[21] This coupling method disappears if the near-surface shear wave speed (V_S) drops below the atmospheric sound speed (Figure 6). Near-surface V_S below that of the speed of sound in air are not uncommon and are often found in regions where the primary surface cover is composed of loose or unconsolidated soil [e.g., Nunziata et al., 2004; Badal et al., 2004; Kanli et al., 2006]. This suggests that the overall paucity of observations of precursory Rayleigh waves may stem from a general prevalence of unconsolidated overburden in the near surface. As the region of the coupling zone (where the excitation condition is met) will be generally narrow and hence close to the projected ground path of a meteor because of the relatively steep inclinations

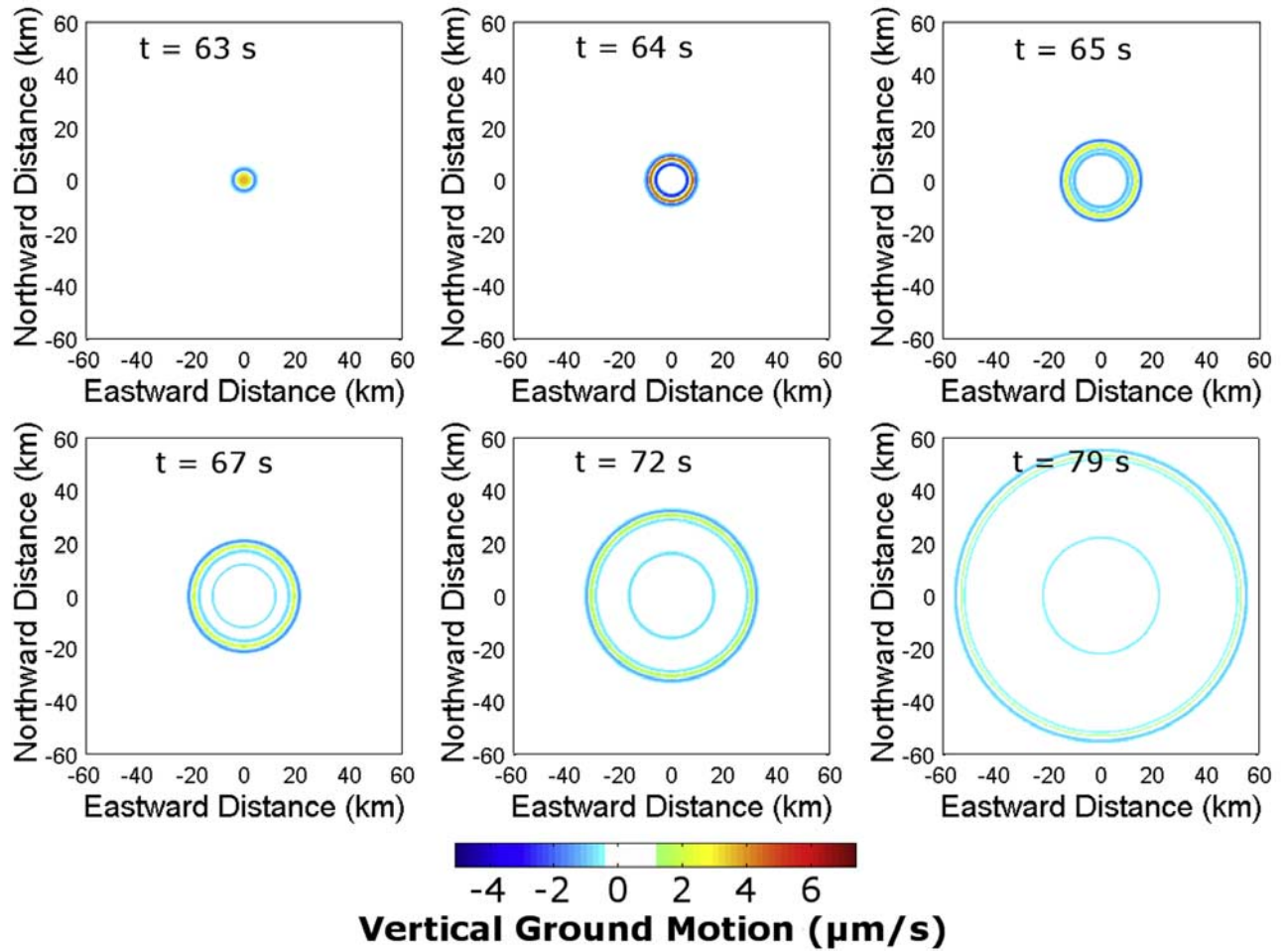


Figure 4. Time slices showing simulation of surface propagation pattern for a granitic surface after an atmospheric point source event at 20 km altitude (similar to a meteoroid terminal burst). Significantly higher amplitude Rayleigh waves (compared to directly coupled airwave) appear to originate from a large ($\sim 10 \text{ km}^2$) circular region ($t = 64 \text{ s}$). In practice, this region would likely appear amorphous in shape, depending upon local surface geology. For a hypersonic shock wave source, this region would be extended along the meteor’s ground-projected trajectory. As time progresses ($t = 65\text{--}79 \text{ s}$) the faster Rayleigh wave velocity, V_R , allows the surface wave to outdistance the slower directly coupled airwave.

required for large P/S velocity materials, the area where such coupling may occur will be small compared to the area over which the airborne wave may be observed. If suitable exposed bedrock or similar high V_S material is not present in this zone, no surface wave or head wave will be generated. Furthermore, scattering of these waves by topographic obstructions (hills, mountains, and valleys) along the path would render the signal more complicated and potentially unrecognizable [cf. *Kanamori et al.*, 1991]. The observations of *Anglin and Haddon* [1987, 1988], where the source meteor passed almost vertically above a seismic array located in flat shield terrain, thus may represent a fortuitous and unusual combination of circumstances.

4.1. Rayleigh Waves

[22] Although rarely observed as precursory waves, Rayleigh waves (a type of seismic surface wave physically similar to wind-driven waves on the surface of a body of water) are a common feature often seen or identified with

meteor seismic recordings. Because of the prevalence of these waves, this section will provide a brief summary of elementary Rayleigh wave theory.

[23] When a wave is incident at a boundary between two media (in this case the air/surface boundary) the wave will reflect and transmit according to Snell’s Law, such that

$$\frac{\alpha}{\sin \theta} = \frac{\alpha'}{\sin R_P} = \frac{\beta'}{\sin R_S} = \frac{1}{p_x}, \quad (2)$$

where θ is the angle of incidence/reflection, R_P/R_S are the angles of refraction for P/S waves (note that in Figure 2 these same angles are $e, e',$ and f'), and $\alpha, \alpha',$ and β' are the acoustic and P and S wave velocities in the air and surface media, respectively. The horizontal component of slowness, or ray parameter, is denoted by p_x . When the angle of incidence reaches a critical angle, the refracted P (or S) wave becomes parallel to the boundary (Figure 7a). Beyond this incidence angle the refracted wave decays exponentially

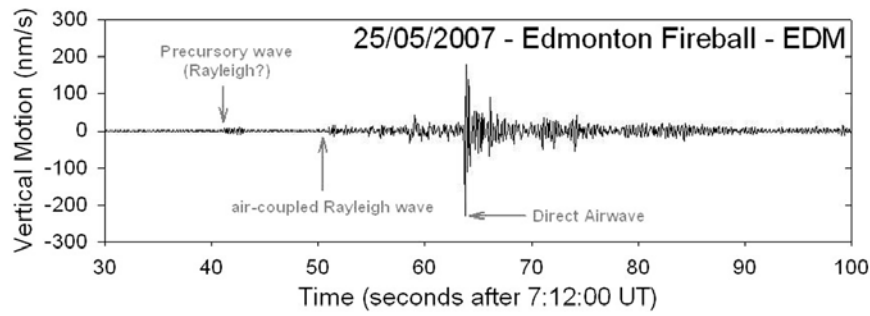


Figure 5. Example of a suspected precursory wave arriving several seconds prior to the wave train associated with the direct airwave from a bright meteor observed near Edmonton, Alberta, Canada, on 25 May 2007 (A. R. Hildebrand, personal communication, 2007). Particle motion suggests this is a precursory Rayleigh wave, yet without a trajectory for the source meteor or a secondary observation to estimate propagation velocity, this identification remains tentative.

away from the interface. A plane wave solution to the wave equation, Φ , then has the form

$$\Phi = A \exp(-\omega p_z z) \exp(i\omega(t - p_x x)), \quad (3)$$

where A is amplitude of the wave, ω is angular frequency, and p_x and p_z are the horizontal and vertical components of the slowness vector, p , respectively. The slowness vector has a magnitude equal to the inverse of the speed and direction perpendicular to the wavefront. This solution represents a type of evanescent wave, which propagates along the interface and decays in amplitude with distance away from the boundary. The Rayleigh wave is a composite wave composed of coupled compressional (P) and vertical shear (SV) evanescent waves. This P/SV wave combination results in the Rayleigh wave having a characteristic retrograde elliptical motion which decays with depth inversely with wavelength, λ . Because of this elliptical motion, these waves are commonly referred to as “ground roll” in exploration geophysics. This retrograde motion continues with depth until the nodal plane, h , is reached at a depth of $\sim\lambda/5$, at which point the motion reverses and becomes prograde (Figure 7b). The Rayleigh wave propagates at a velocity, V_R , which is slightly slower than the shear wave velocity, V_S . For example, in a Poisson solid ($V_P/V_S = \sqrt{3}$), V_R is $\sim 92\%$ of V_S . In addition, Rayleigh waves are polarized, with particle motion confined to a plane pointing back toward the source [Ewing et al., 1957; Aki and Richards, 2002].

[24] In the simple case of an infinite half-space (the ground) bounded by a free surface (where the displacement is unconstrained and the stresses vanish), the Rayleigh wave behaves as described above with no dispersion. However, in the more general case when the surface is a layered medium, dispersion of the Rayleigh wave train occurs. Since seismic wave velocities generally increase with depth and long-wavelength Rayleigh waves are more sensitive to deep-seated layers than short-wavelength Rayleigh waves, the nature of the dispersion is usually such that long-wavelength waves have a higher phase velocity. This results in a phase velocity curve similar to Figure 7c. The group veloc-

ity, v_g , at which the energy at these wavelengths propagates, is related to the phase velocity by the relationship

$$v_g = \frac{v}{1 - \frac{\omega}{v} \frac{\partial v}{\partial \omega}}. \quad (4)$$

[25] The case where $v > v_g$ is “normal dispersion” (longer wavelengths or periods arriving before shorter), whereas the case where $v < v_g$ is “anomalous dispersion” (shorter before longer). An important feature of the group velocity dispersion curve is the existence of a local minimum velocity, which produces a discrete arrival called an

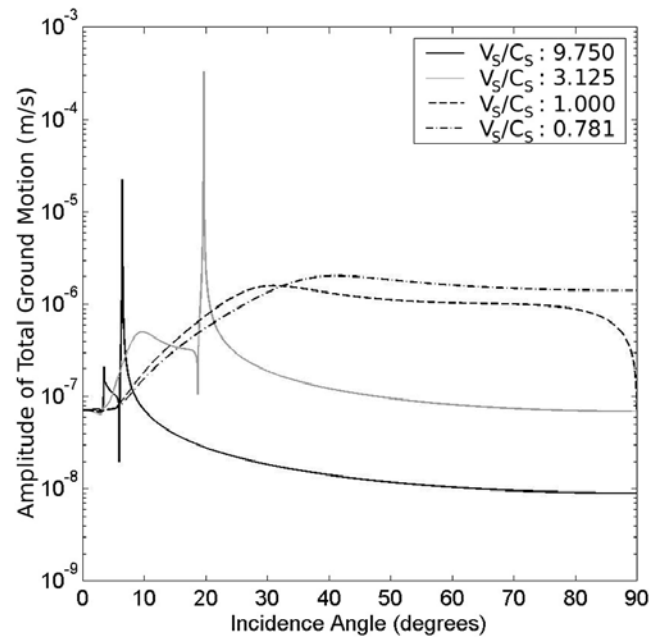


Figure 6. Amplitude behavior of observed seismic coupling as the shear wave velocity is gradually lowered below the atmospheric sound speed, C_S . Note that the P wave velocity is held fixed in these examples for illustrative purposes.

Airy phase (Figure 7c). Since frequencies close to this minimum propagate at the slowest velocities, they arrive last and terminate the dispersive Rayleigh wave train, often with significant energy and amplitude. The Rayleigh wave

train may also contain regular harmonics with significant amplitude. It is also notable that the second type of surface wave, the Love wave (consisting of evanescent SH waves), in an ideal homogeneous medium, will never be generated by meteor-related seismic signals since acoustic waves cannot produce transverse motion in the surface because of the atmosphere’s inability to support shear waves. In reality, the surface is rarely ideal, and heterogeneities in the surface will result in the scattering of the induced surface wave, producing a mixture of P/SV and SH waves [e.g., Langston, 2004]. For a more complete elaboration of the theory for layered media, the reader is referred to Ewing et al. [1957].

4.2. Air-Coupled Rayleigh Waves

[26] Classical Rayleigh wave theory derives from treatment of Earth’s surface as a free surface. On the other hand, if the acoustic properties of the air are explicitly considered, theoretical treatments of the problem predict the existence of air-coupled Rayleigh waves [Ewing et al., 1957; Langston, 2004]. This type of wave was first described and theoretically explained for layered media by Press and Ewing [1951] after observations of extended sinusoidal wave trains during seismic exploration tests using elevated sources. Consisting of a train of dispersive (though nearly constant frequency) waveforms that follow the airwave arrival, these waves are generally characterized by retrograde elliptical motion similar to classical Rayleigh waves (Figure 8). The propagation of these waves is heavily dependent upon the shear velocity in the near surface [Ewing et al., 1957; Langston, 2004]. Where the target surface’s group velocity is slower than the apparent horizontal velocity of the airwave over the surface, these air-coupled surface waves lag behind the coupled airwave, while if v_g is greater, they will precede it [e.g., D’Auria et al., 2006] (Figure 5). As discussed at the end of section 4.1, if the shear velocity exceeds the atmospheric acoustic speed too greatly, Rayleigh wave production is decoupled from the airwave. In the case of meteor-related seismic observations, air-coupled Rayleigh waves generally follow immediately after the coupled airwave, which quite often is associated with a ballistic shock (Figures 8 and 9). Retrograde motion is most common, but prograde motion has also been observed [e.g., Langston, 2004]. The air-coupled Rayleigh waves are effectively “attached” to the airwave as

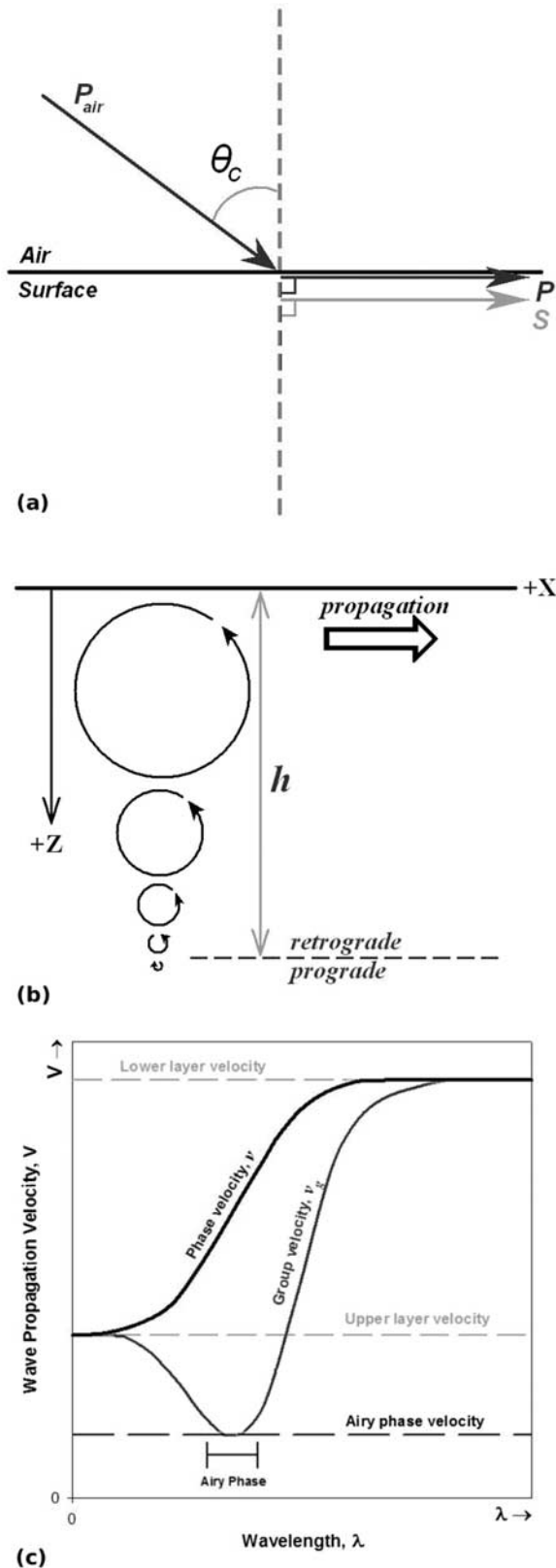


Figure 7. Characteristic properties of Rayleigh waves at an air-ground contact. (a) Incident wave geometry at the fluid/solid contact for generation of surface waves. (b) Retrograde elliptical motion of the Rayleigh wave, polarized toward source. Note amplitude decay with increasing depth. Propagation velocity, V_R , is slightly less than the shear velocity, V_S , of the surface. (c) For a layered surface the Rayleigh wave becomes dispersive. Normal dispersion refers to the case where $v > v_g$, whereas anomalous dispersion refers to the case where $v < v_g$. As wavelength increases, v varies from upper to lower layer velocities. In general, v_g displays a minimum that is associated with an Airy phase.

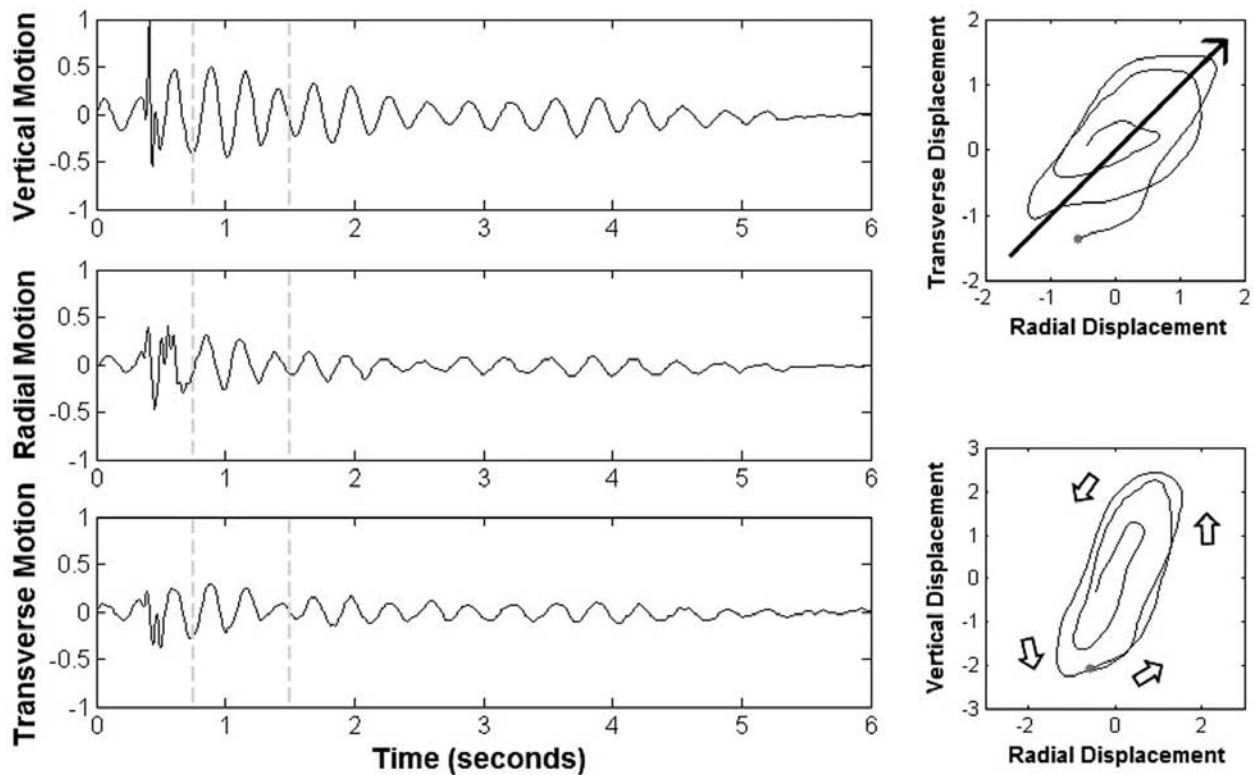


Figure 8. Example of an air-coupled Rayleigh wave from a 5 pound (~ 2.3 kg) explosive charge elevated at 10 feet (~ 3 m) above the ground, after *Press and Ewing* [1951]. This source produces polarized, retrograde elliptical motion similar to conventional Rayleigh waves. (left) Particle motions correspond to (right) time interval between dashed lines. Amplitudes have been normalized to peak vertical motion.

it moves along the surface. After passage of the airwave, the air-coupled Rayleigh wave gradually decays, often persisting for tens of seconds to a few minutes. Finally, as is the case for classical Rayleigh waves, harmonics (higher-order modes) may be present, and surface layering will tend to produce strong dispersion. Examples of these waves with these characteristics are shown in Figure 9 and later in section 6.

5. DIRECT AIRWAVE COUPLING

[27] By far, the most commonly observed seismic recordings are those that involve direct coupling of the airwave with the ground. These observations are most often identified by the coincident appearance of tremor-like signals on local seismographs soon after a visual observation of a meteor/fireball/bolide [e.g., *MacCarthy*, 1950]. Often exhibiting the generally slow apparent velocities consistent with propagating atmospheric acoustic waves [e.g., *Aikman et al.*, 1989], the coincident appearance of weak seismic signals at expected arrival times for acoustic waves led early investigators to use these as constraints on the locations of potential meteorite strewn fields [*Folinsbee et al.*, 1967, 1969; *Cevolani et al.*, 1994].

[28] Directly coupled airwaves show several distinctive characteristics. First, they tend to be short in duration, lasting from several seconds to approximately a minute.

These waves also lack distinct P and S wave arrivals characteristic of a local earthquake (Figure 9). With spectral content typically peaking at frequencies of ~ 0.1 – 10 Hz the seismic recordings of directly coupled airwaves reflect the characteristics of the incident wave [*ReVelle*, 1976; *Edwards et al.*, 2007]. Finally, seismic recordings associated with ballistic shocks typically display downward first motions and W-shaped pulses [*Kanamori et al.*, 1991, 1992; *D’Auria et al.*, 2006]. The distinctive W-shaped pulse occurs since the velocity response of seismometers is approximately proportional to the time derivative of the N-shaped acoustic pulse [*Beyer*, 1997, pp.189–196]. The downward first motion reflects overpressure of the first arrival of the acoustic wave (Figure 9).

[29] Although plagued by a paucity of seismic recordings and often only eyewitness or solitary camera observations of the meteor itself, some of the earlier events cited above revealed that acoustic sources could be classified according to two distinct mechanisms: (1) the nearly cylindrical hypersonic shock or ballistic wave produced by the high-velocity motion of the meteoroid through the atmosphere and (2) the catastrophic fragmentation or disruption experienced by some meteoroids, often termed terminal bursts or flares, due to the proximity of these events to the end of the luminous part of the trajectory.

[30] For the most part, the value in these recordings lies in their kinematic information. Since they record the arrival

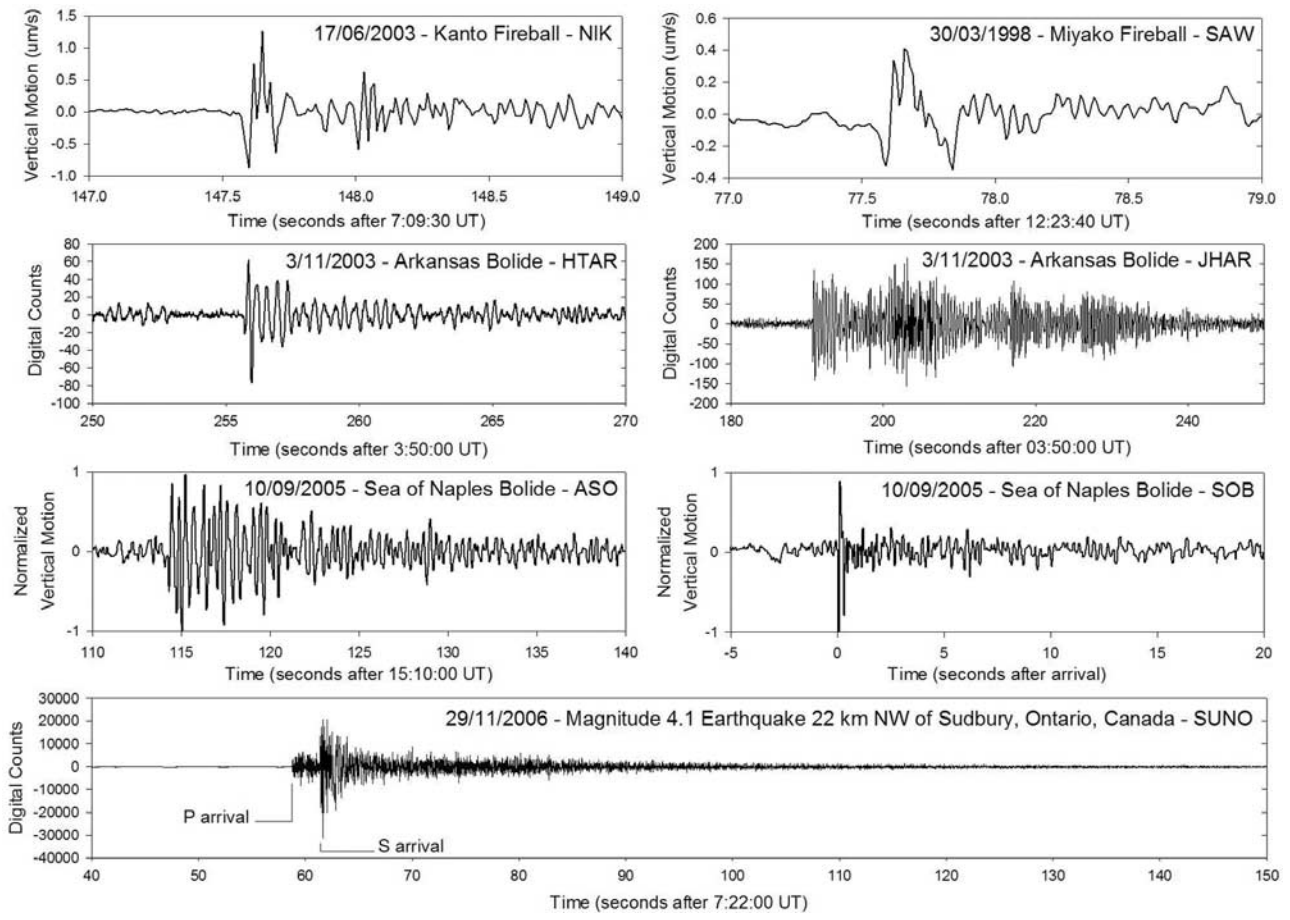


Figure 9. Examples of seismic waveform recordings of meteor-generated ballistic shocks. Note the dissimilarities in duration and structure to that of a local earthquake.

times of the incident airwaves at the position of the seismic station, they can be used directly for trajectory reconstruction (see section 5.1). This is by far the most common analysis performed from seismic meteor recordings to date, as this information is the easiest to measure and interpret. Nevertheless, the coupling of airwave into the ground can be quantified. The simplest approach approximates the atmosphere/surface boundary as fluid/solid half spaces in contact, where vertical displacement and stress are continuous across the interface, while shear stress across the interface is zero (Figure 2). In this case, the following relationships apply to the transfer from acoustic to seismic wave motion in the surface [Ben-Menahem and Singh, 1981, 2000]:

Radial motion

$$v_x = P_0 \frac{\cos e \sin(e' - 2f')}{\rho' \alpha' m_1} \exp(i\chi) \quad (5)$$

Vertical motion

$$v_z = -P_0 \frac{m_2 \cos e}{\rho \alpha m_1} \exp(i\chi), \quad (6)$$

where

$$m_1 = \cos e \left[\left(\frac{\beta'}{\alpha'} \right)^2 \sin 2e' \sin 2f' + \cos^2 2f' \right] \quad (7)$$

$$m_2 = \left(\frac{\rho \alpha}{\rho' \alpha'} \right) \cos e'. \quad (8)$$

Here e , e' , and f' are the angles of incidence of the airwave and refraction of the P and S waves, respectively, while α and ρ and α' and ρ' are the V_P and densities for the fluid and solid half-spaces, respectively, and β' is the shear velocity or V_S in the solid half-space (Figure 2). Note that in the fluid half-space, $\beta = 0$ m/s. These expressions reduce to the following forms in cases of grazing or postcritical incidence [Ben-Menahem and Singh, 1981, 2000]:

Radial motion

$$v_x = \frac{P_0 \hat{c}}{2(\lambda + \mu)} \exp(i\chi) \quad (9)$$

Vertical motion

$$v_z = P_0 \frac{\hat{c} e^{-i\pi/2}}{2(\lambda + \mu)} \left(\frac{V_P}{V_S} \right)^2 \exp(i\chi), \quad (10)$$

with

$$\chi = \omega \left(t - \frac{x}{\hat{c}} \right) \quad (11)$$

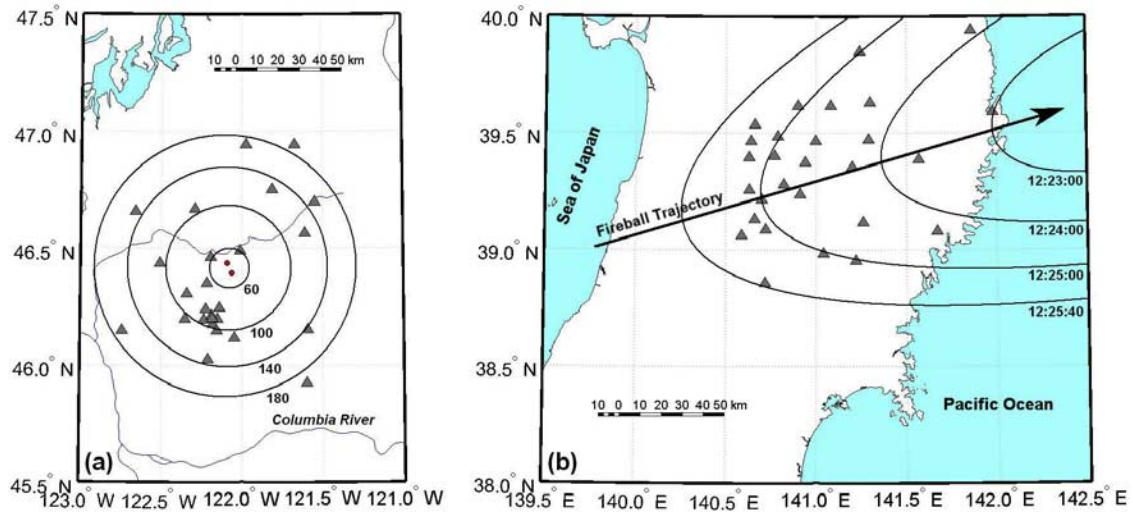


Figure 10. Schematic diagrams of the arrival time distributions associated with two meteor-related seismic events over two different regional seismic networks. (a) Arrivals associated with two fragmentation events or terminal airbursts near Mount Adams, USA, in 1989 [from *Qamar*, 1995] and (b) arrivals associated with a meteor’s ballistic shock wave near Miyako, Japan, in 1998 [from *Ishihara et al.*, 2003a].

and

$$\hat{c} = \frac{C_S}{\sin e}, \quad (12)$$

where P_O is the overpressure (or amplitude) of the incident airwave, V_P , V_S , λ , and μ are the compressional and shear wave speeds and the associated Lamé parameters of the surface layer, respectively, and \hat{c} is the trace velocity of the acoustic wave. C_S and e are the acoustic wave speed of the air and the incidence angle of the airwave, measured from the vertical. In practice, equations (9)–(12) are generally applicable at angles beyond critical incidence, since beyond the Rayleigh critical angle the general expressions (equations (5)–(8)) are slowly varying and (where $V_S < C_S$) nearly constant (Figures 3 and 6) [e.g., *Langston*, 2004]. It is also noted that the Earth’s atmosphere favors the observation of grazing or near-grazing incidences in comparison with a constant velocity medium, as the acoustic wave will refract in the troposphere back toward the stratosphere as the observer’s range increases.

[31] Despite their simplicity, the acoustic-seismic coupling expressions above have successfully reproduced the basic structural response of the initial coupled shock wave observed for several seismically recorded meteor [*Langston*, 2004; *D’Auria et al.*, 2006] and high-velocity artificial shock waves [*Kanamori et al.*, 1992; *Edwards et al.*, 2007]. Some theoretical and empirical results even show that the magnitude of the coupling predicted by these expressions, in particular for grazing incidence, is accurate to within a factor of <3 of the actual observations [*Kanamori et al.*, 1992; *Edwards et al.*, 2007]. As will be discussed in section 7, this may provide a basis for a general meteor magnitude scale, as well as a point of comparison with other, more detailed, methods of coupling. Yet despite these positive results, simple half-space coupling does not reproduce the long enduring wave trains

of air-coupled Rayleigh waves often induced by the incident shock wave, as this model ignores any deeper geological structures at the observation site. To reproduce these wave train observations, layered media are often more appropriate and successful [e.g., *Langston*, 2004; *Edwards et al.*, 2007].

5.1. Trajectory Reconstruction

[32] As global seismic monitoring has spread, multiple seismic observations of individual meteor events have become more common. Mapping of arrival times has allowed the two mechanisms (cylindrical versus point source) to be more easily distinguished (Figure 10), enabling inversion for meteor path and/or fragmentation location. Inversion of suspected meteor-related seismic arrivals was first attempted by *Nagasawa* [1978] to reconstruct the trajectory of a meteor observed over the Kanto Plains in Japan. Since then, a number of authors [*Nagasawa and Miura*, 1987; *Ishihara et al.*, 2003a, 2004; *Brown et al.*, 2003; *Tatum et al.*, 2000; *Langston*, 2004; *Pujol et al.*, 2005, 2006] have pursued trajectory reconstruction with seismic observations using several variations of the same technique. The essence of the technique involves using the observed seismic times of arrival at the surface to constrain the location and orientation of the hypersonic shock of the source meteor at altitude.

[33] Much like supersonic aircraft, meteors produce a conical shock front or Mach cone due to their faster-than-sound velocities. Since meteor velocities are significantly faster than aircraft, the angular width or Mach angle, β , of the cone is significantly smaller of order a degree (Figure 11) and varies according to

$$\sin \beta = \frac{C_S}{v} = \frac{1}{M}, \quad (13)$$

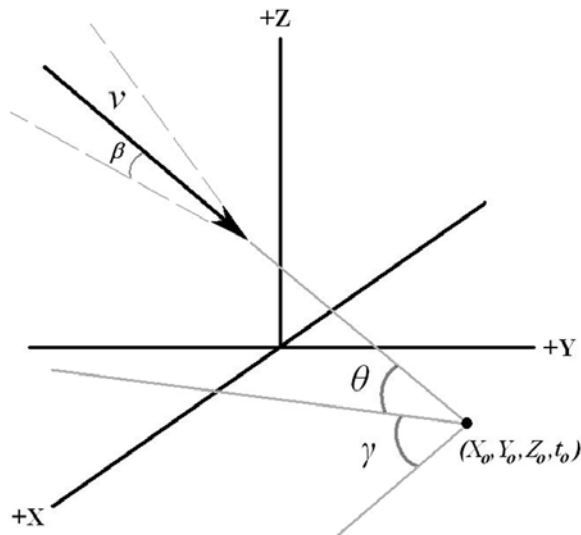


Figure 11. Schematic diagram of the orientation of a meteor trajectory and its associated fitting parameters, as defined by Ishihara et al. [2003a]. Parameters γ and θ , the azimuth and elevation angles, respectively, define the orientation of the trajectory, fixed at a position (X_o, Y_o, Z_o) in the local coordinate frame (note that often $Z_o = 0$). The meteor’s velocity, v (a proxy for Mach cone angle, β), determines the time, t_o , of this intersection.

where C_S is the speed of sound in air, v is the velocity of the meteor, and M is the Mach number or the ratio of v to C_S .

[34] The narrowness of the Mach cone coupled with the high altitude of the meteor mean that the highly nonlinear region of the shock cone never reaches the surface directly; instead, it propagates outward at acoustic velocities to the surface. Fitting of the six free parameters that define the meteor trajectory becomes a geometrical inversion problem constrained by the traveltimes of the conical wavefront to each observing station. The six free parameters that characterize the trajectory are as follows from the definition of Ishihara et al. [2003a] (Figure 11):

- X_o, Y_o horizontal coordinates of the trajectory intersection with the surface ($Z_o = 0$);
- t_o time of intersection of meteor trajectory at $(X_o, Y_o, 0)$;
- γ azimuth of the trajectory;
- θ elevation angle of the trajectory relative to the horizon;
- v velocity of the meteoroid.

[35] The traveltime from this generalized meteor Mach cone to an arbitrary station at the surface is then given by [Ishihara et al., 2003a; Pujol et al., 2005]

$$t = t_o + \frac{1}{v} \left(\frac{x_{\perp}}{\tan \beta} - x_{\parallel} \right), \quad (14)$$

where x_{\perp} and x_{\parallel} are the distances of the station perpendicular and parallel to the trajectory, respectively. The derivation of equation (14), along with a detailed description of the problem, is given by Pujol et al. [2005].

Thus given a sufficient number of observations at the surface, the six free parameters that define the meteor trajectory may be solved for by minimizing the residuals in either an L1,

$$R = \sum_n |t - t_{obs}|, \quad (15)$$

or L2 norm,

$$R = \sum_n (t - t_{obs})^2, \quad (16)$$

where t and t_{obs} are the computed and measured signal arrival times. Minimizing this residual function has been accomplished primarily using massive grid searches of the parameter space [e.g., Nagasawa and Miura, 1987; Ishihara et al., 2003a]; however, recent development of an iterative inverse method by Pujol et al. [2005] is becoming more commonly used [D’Auria et al., 2006; Dailu and Yarong, 2007].

[36] In practice, of the six free parameters, the four that define the orientation of the trajectory (X_o, Y_o, γ , and θ) are generally well resolved [cf. Ishihara et al., 2003a; Langston, 2004; Pujol et al., 2006], while the remaining two, v and t_o , have been found to be more difficult to

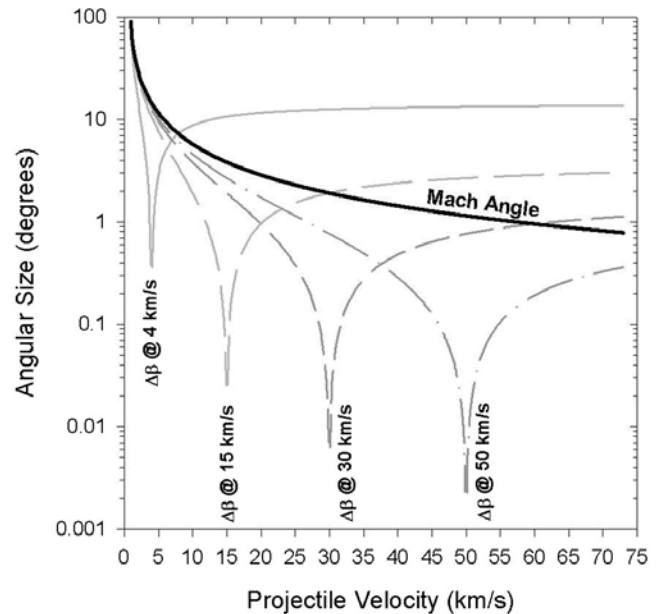


Figure 12. The Mach cone angle (solid line) and changes in Mach cone angle as a function of velocity (gray dashed lines). The angular size of the Mach cone, β , decreases rapidly with increasing velocity from the supersonic regime ($M < 5$) of high-speed aircraft to the hypersonic regime ($M > 5$) typical of meteors. Differences in Mach angles, $\Delta\beta$, at low velocities tend to be large and so are more easily resolved by seismic traveltime inversion. At higher velocities these angular differences become increasingly subtle leading to large uncertainties in velocity during inversion. Distinguishing between such high velocities requires extremely accurate traveltime observations.

constrain and are highly sensitive to initial assumed values [Pujol *et al.*, 2005]. Implicit in equation (14) is the commonly used assumption of a constant speed of sound or isothermal atmosphere. This assumption simplifies the geometric rays, which would otherwise curve because of atmospheric refraction [Tatum, 1999], to straight lines allowing for rapid traveltimes calculation. The drawback to this assumption is that because C_S is a fundamental part of the geometric definition of the Mach cone (equation (14)), the meteor velocity, v , becomes dependent upon the choice of C_S . Additionally, because the time of intersection at the surface, t_0 , depends upon the meteor's velocity, it too becomes dependent upon the chosen model's value of C_S . The way around this dependency is to set aside isothermal/constant C_S assumptions for the atmosphere and adopt an inhomogeneous atmospheric model constrained by meteorological data of upper atmospheric temperature. The tradeoff for this approach is an increase in the complexity of the problem, as rays will then refract and Mach cone geometry becomes variable with altitude. These complications contribute to the inversion procedure becoming more computationally intensive.

[37] Another reason for the difficulty in resolving meteor velocity is that the geometry of the Mach cone does not vary greatly over the wide range of possible meteor velocities (Figure 11). This small variation is likely the source of large upper bound uncertainties in velocity obtained by this method [Ishihara *et al.*, 2003a, 2004]. Such small variations in the angular extent in the Mach cone result in smaller and smaller changes in traveltime as the meteor velocity increases. For example, the traveltime for a station located 200 km from the X_o , Y_o intersection, vertically beneath a meteor at 45° inclination (for simplicity), for a slow 12 km/s meteor is 650.89 s (equation (14)). For a somewhat faster meteor at 20 km/s the traveltime becomes 655.76 s, a difference of only 4.87 s. Yet this same small change in traveltime encompasses nearly all of the remaining 85% of the meteor velocity range (11.2–72.8 km/s) if applied at 20 km/s. Typical event residuals currently reside at about 10% of this difference, at ~ 0.5 s or greater [cf. Ishihara *et al.*, 2003a; Pujol *et al.*, 2006], while arrival time uncertainties generally are smaller at <0.1 s but may exceed 1 s at times [e.g., D'Auria *et al.*, 2006] depending upon the clarity of the seismic response to the airwave.

[38] The end result of such small changes in traveltime is that the ability to distinguish the fine changes between one Mach cone (or velocity) from another requires a high degree of precision in traveltime calculations during inversion for high-velocity meteors (Figure 12). As the acoustic wave velocity depends significantly on atmospheric conditions at the time of a fireball event, precise timings are possible only with detailed knowledge of these conditions. Such meteorological details of upper atmosphere are simply not known to the level of precision needed to resolve extremely high velocity events. Yet approximations to the actual profile (such as smoothing or constant velocity assumptions) appear to be adequate to resolve lower-velocity events such as supersonic aircraft or the lower range of meteor velocities

(~ 20 –11.2 km/s). This suggests that meteor velocities beyond ~ 20 km/s may not be resolvable by seismic methods. Despite this limitation, the ability to determine meteoric trajectories solely by seismic arrival time inversion is potentially very useful, for example, by providing investigators with a constraint for the location of potential meteorites on the ground where little or no visual records of the meteor exist.

[39] Confirmation of the inversion method's abilities has been made by applying seismic trajectory inversion to the 6 May 2000 Moravka meteorite fall in the Czech Republic, where an independent solution from video records exists [Brown *et al.*, 2003; Pujol *et al.*, 2006]. In this instance, the entry angles and azimuths determined from the seismic solution were on the order of a few degrees from the video result, providing some measure of the accuracy expected in the seismic solution of fireball trajectories. As expected, the velocities estimated by the seismic technique (8.3 km/s for Brown *et al.* [2003] and 12–21 km/s for Pujol *et al.* [2006]) were lower than the measured video initial velocity of 21.9 km/s, emphasizing the large uncertainties in seismic determinations of meteor velocity.

5.2. Aerial Point Source Location

[40] The second mechanism producing meteor-related seismic observations, meteoroid fragmentation, is geometrically simpler than that of ballistic wave observations. In these cases, quasi-point-like impulsive airborne shock waves are produced during a meteoroid's descent as the object breaks up suddenly because of the increasingly large ram air pressure acting upon it during entry. These energetic events are often characterized optically by a brief ($\ll 1$ s), yet dramatic, increase in the brightness of the meteor. Physically, this is the result of the meteoroid shattering into fragments, which exposes a larger surface area to the oncoming air stream, increasing the rate of ablation and thus the amount of light produced [Ceplecha *et al.*, 1998]. Such kinetic explosions may result in separation of the original body into several large fragments, each of which may then continue to ablate separately (gross fragmentation), or complete disintegration of the meteoroid into fine dust [e.g., Klekociuk *et al.*, 2005]. The phenomena in the latter case are often referred to as “flares,” “terminal bursts,” or simply “airbursts.”

[41] As these explosive fragmentation events are very brief and take place over small portions of the entire meteor trajectory, they are often approximated by a point source, though in reality the source may be somewhat elongated along the direction of travel. Therefore atmospheric shock/acoustic/infrasonic waves that originate from these sources, along with their observed air-coupled seismic counterparts, can be distinguished from ballistic waves by propagating outward quasi-spherically. This characteristic results in a circular symmetry for the arrival pattern at the surface (Figure 10b). Inversion of these types of observations takes a form equivalent to earthquake location, either using preexisting earthquake hypocenter programs and appropriately modified Earth models to account for the much slower

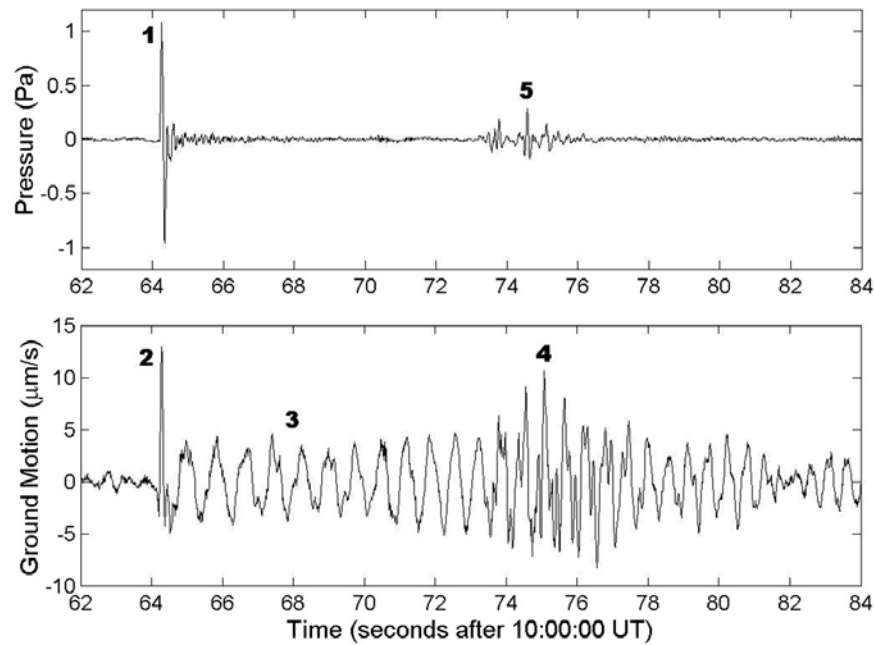


Figure 13. Simultaneous colocated (top) infrasonic and (bottom) seismic observations of the NASA Stardust sample return capsule shock wave, 15 January 2006. At point 1, the initial airborne shock wave arrives at the sensor site. At point 2, the shock wave directly couples to the ground (a clay playa) producing a W-shaped impulse. At point 3, the coupled shock wave generates an air-coupled Rayleigh wave in the playa, which persists for approximately 1 min. At point 4, layering in the subsurface causes dispersion of the Rayleigh wave punctuated by the arrival, ~ 10 s after the shock wave, by an Airy phase. At point 5, arrival of this Airy phase is recorded infrasonically as the ground motion couples back into the air.

atmospheric signal speed [e.g., *Johnston, 1987; Qamar, 1995*] or using similar reduction techniques and full atmospheric ray tracing techniques [e.g., *Edwards and Hildebrand, 2004*]. Regardless of the specific implementation, however, the point-like nature of the source results in an inversion for only the source's 3-D position, X , Y , Z , and the associated time of occurrence, t_o . Similar to trajectory inversion, the solution to this problem requires minimization of the traveltimes residual, with the additional constraint that t_o for the event is the same for all observations. A solution is obtained by minimizing either the L1 residual, namely,

$$R = \sum_n |t_{obs} - t - t_o|, \quad (17)$$

or the L2 residual,

$$R = \sum_n (t_{obs} - t - t_o)^2, \quad (18)$$

where t_{obs} are the observed times of arrival of the seismically detected airwave and t are the computed traveltimes at each station from a point source located at X , Y , Z .

[42] We remark that location of a single fragmentation event is not sufficient to compute the full trajectory of the meteor [e.g., *Arrowsmith et al., 2007*]; however, in cases where several point source-type events occur along a meteor's path [e.g., *Qamar, 1995; Brown et al., 2003*,

rough trajectory information may be gleaned. As in the case of ballistic trajectory reconstruction, there are substantial uncertainties associated with the estimation of meteor velocity using this approach.

6. DYNAMICS OF DIRECT AIRWAVE COUPLING

[43] The increasing number of observations of naturally occurring meteor airwaves coupling with the surface under a variety of geographic and geologic settings (Tables 1a and 1b) raises questions about what surface conditions are conducive to surface coupling. Previously, it has been shown that in cases where the surface shear velocity is lower than the speed of sound in air, not uncommon for unconsolidated soils, the coupling of waves from the air into the ground is more effective as the incident airwaves refract downward into the surface [*Langston, 2004*]. Recent colocated infrasonic/seismic observations of the shock wave from reentry of NASA's Stardust sample return capsule [*Edwards et al., 2007*] provides an example for which coupling efficiency has been measured directly. This hypervelocity reentry of a well-calibrated meteor analog produced a low-frequency shock wave at high altitudes, similar to that of natural meteors. At an initial velocity of 12.5 km/s, the capsule was equivalent to a slow moving meteor, with the benefit of having known physical properties (mass, volume, shape, and density) prior to reentry [*ReVelle and Edwards, 2007*]. Such parameters generally remain unknown or poorly constrained for natural meteors [*Ceplecha et al.,*

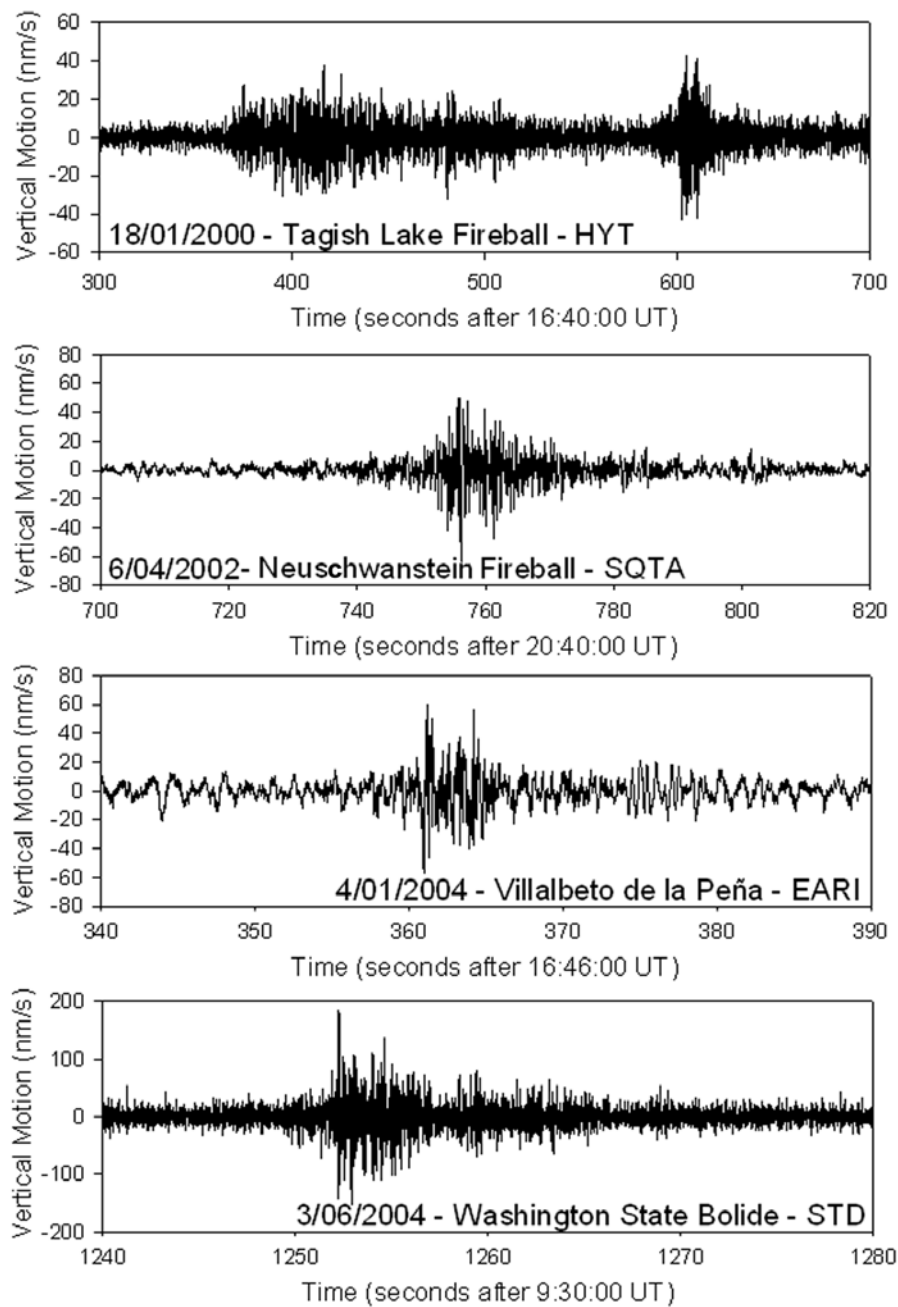


Figure 14. Examples of meteor-related air-coupled seismic signals displaying a dispersed pulse shape. Typically, these occur from fragmentation or terminal airbursts of a meteoroid, but some instances exist (e.g., Neuschwanstein, SQTA) that appear to originate from ballistic waves [ReVelle *et al.*, 2004].

1998]. In terms of energy, the acoustic-seismic coupling efficiency for the clay-rich playa at the observation location was determined to be $\sim 2\%$ (10^{-2}), significantly higher than previously employed estimates of 10^{-4} or 10^{-7} [Brown *et al.*, 2002b] and somewhat higher than those predicted from simple welded acoustic/elastic boundary approaches (equations (5)–(12)).

[44] The seismic records of the Stardust sample return capsule reentry also contained air-coupled Rayleigh waves with a complex character. Time-frequency analysis of these waves revealed signals interpreted as fundamental and higher-order Rayleigh wave modes, terminated by promi-

nent Airy phases. The Airy phases were also detected by the infrasound sensors (Figure 13), providing evidence for “reverse” coupling from ground into the air. The infrasonic signals of the late-arriving Airy phase had previously been interpreted to be the likely result of atmospheric multipathing [ReVelle and Edwards, 2007], although no satisfactory atmospheric model was found to explain the arrival. Furthermore, on the basis of previous examples cited above, had this been a natural meteor it is possible that the late arrival could have been misinterpreted as a fragmentation event. This example illustrates the importance of understanding the complexities of air-ground interaction, partic-

ularly where unconsolidated near-surface layers are present. Still more complexities in the observed waveform can arise if site-specific sources of scattering or reflection are nearby, such as mountains, large buildings [e.g., *Kanamori et al.*, 1991], or geologic boundaries.

[45] In addition to air-coupled Rayleigh waves, some signal traits of seismic observations of meteoroids that have terminated in “explosive” events remain poorly understood. In general, observations of these point source-like events tend to be diffuse, with no distinct arrival time, in contrast to the often sharp onset of ballistic observations. These signals generally ramp up, peaking at some maximum value before decaying back to presignal levels (Figure 14). Although these signals may be complicated by local site conditions, their systematic association with explosive events suggests that their diffuse character primarily reflects fragmentation processes. More study is needed to gain a better understanding of the phenomenon.

7. FUTURE DIRECTIONS

[46] The rising number of recorded meteor-related seismic observations (Tables 1a and 1b) has resulted in refinements to methods of determining locations and trajectories of the source meteoroids. Earlier massive parameter grid searches of *Nagasawa* [1978] and *Ishihara et al.* [2003a] have been improved upon using linearization techniques for simple model atmospheres [*Pujol et al.*, 2005]. Somewhat more slowly, the variability of the atmosphere and upper air winds on wave propagation are being incorporated into solutions, as the directional anisotropy induced by the presence of winds can introduce substantial shifts in the final solution on the order of several kilometers [*Edwards and Hildebrand*, 2004; *D’Auria et al.*, 2006]. Incorporation of meteorological and upper air data should become easier as the availability of regional and global meteorological data/models also increases.

[47] Beyond further refinements in the methodology of how these locations and trajectories are determined, available techniques still provide only a positional constraint on the source. Can seismic observations of meteors provide information about the associated meteoroids, even in cases where only a solitary observation is made? Or, more simply, can a seismic meteor magnitude scale be established to enable estimation of the source meteor’s energy from a solitary observation? The answers to these questions require a detailed understanding of how atmospheric waves couple with Earth’s surface in a wide variety of geological settings. This remains an area of active research because of the complexity of the more general problem.

[48] In order to understand the air-ground coupling phenomenon more completely, it has been suggested [*Edwards et al.*, 2007] that we appeal to a microphysical view of these porous surfaces pioneered by *Biot* [1956a, 1956b]. Biot theory, refined later by *Stoll* [1980] for ocean sediments, treats the subsurface as a mixture of solid and fluid media, with a fluid-filled pore space surrounded by a solid framework that is the matrix of the soil. Within this composite

material, three distinct types of waves propagate: two compressional waves and a shear wave. The compressional wave of the “first kind” is effectively an elastic P wave that propagates primarily through the solid grains; similarly, the shear wave is an elastic S wave that also propagates through the solid framework. A compressional wave of the “second kind” travels more slowly than the first and is highly attenuated, propagating primarily through the pore space fluid, be it air, water, or some other fluid [*Sabatier et al.*, 1986]. Despite its high degree of attenuation, the compressional wave of the second kind may lead to enhanced air-ground coupling since it provides a mechanism for atmospheric waves to interact with the much larger effective surface area than the planar ground surface. This microphysical view may help to explain the wide variation in observations of acoustic coupling efficiency (10^{-2} to 10^{-7}) discussed previously in section 6, as hard, consolidated rocks often have low porosities, limiting coupling of an atmospheric wave to just the exposed surface.

[49] In contrast to the acoustic-seismic transfer process, in meteor-generated infrasound theory it is well established that an observation of the airwave (ballistic or ablatational) can provide fundamental constraints on the energy of the source meteoroid under certain simplifying assumptions. For example, the fundamental period of an acoustic/infrasonic observation is related to the size of the blast cavity that produced the airwave initially (with a degree of range dependence). In the case of ballistic waves this is the radius, R_o , of the nearly cylindrical cavity associated with highly nonlinear wave propagation region produced by the shock of the meteoroid’s passage through the atmosphere. This is often referred to as the “blast radius” and is related to the fundamental frequency, f_m , by the quasi-empirical relation

$$f_m = \frac{C_S}{2.81R_o},$$

where

$$R_o = \left(\frac{E}{\pi p_o L} \right)^{1/2}. \quad (19)$$

In the case of fragmentation or quasi-spherical point source events the fundamental frequency is related to a similar radius, with an approximately spherical geometry, namely,

$$f_m = \frac{C_S}{2.21R_o},$$

where

$$R_o = \left(\frac{3E}{4\pi p_o} \right)^{1/3}, \quad (20)$$

where C_S is the ambient thermodynamic sound speed at the source, p_o is the ambient pressure at the source altitude, L is the length of the meteor’s trajectory, and E is the portion of the meteor’s energy producing the shock wave [*ReVelle*, 1974]. We remark that these relations apply in the immediate vicinity of the nonlinear blast zone; at the

surface the period and amplitude observed are modified from these initial values through attenuation, shock effects with long-range propagation, and the winds/temperature structure of the atmosphere between the high-altitude source and low-altitude receiver.

[50] Through the fundamental frequency, the amount of energy deposited in the atmosphere per unit length of trail required to produce such an acoustic response may be estimated using knowledge of the ambient pressure and sound speed at the source region (which may be established through ray tracing). Using this energy, an estimate of the acoustic efficiency, some assumptions or measurements of the meteoroid's velocity, v_m , and density, ρ_m , and a further estimate of the size of the meteoroid can also be made. Knowing the sizes of the source meteoroids, the frequency of their detection, and an estimate of the global coverage monitored, one can calculate the flux of these objects at the Earth, a major goal of meteor science. The flux of larger (meter-sized) meteoroids at the Earth is still poorly known [cf. *Brown et al.*, 2002a]. The flux of projectiles in this size range is crucial for interpreting the young surfaces of asteroids, several of which have shown a large deficit of small craters [*Chapman et al.*, 2002]. Given the global distribution of seismograph networks, what is particularly encouraging about seismic detections of meteoroids is their potential to estimate this flux independently of other techniques.

[51] Our current understanding of meteor-related seismicity is still far from this ultimate goal, however. Estimates of meteoroid energy from seismic data have been attempted in the past [e.g., *Brown et al.*, 2002b, 2004; *Llorca et al.*, 2005], with limited success, using the empirical energy relationship derived from the mining and surface explosions work of *Gupta and Hartenberger* [1981]. The relationship, modified for use with the higher-altitude meteor sources, relates the equivalent energy yield, W , in kt of equivalent TNT (1 kt of TNT = 4.185×10^{12} J) to the observed vertical seismic motion, D_V (nm/s):

$$W = \frac{\chi R^2 (2.748 \times 10^{-7} \alpha D_V)^{1.738}}{\gamma}. \quad (21)$$

Here R is the range to the source event in meters and α , χ , and γ are the added terms accounting for air-to-ground coupling efficiency, coupling efficiency scaling from near-surface explosions to high-altitude sources, and surface wave attenuation for different surfaces, respectively. Although using rough estimates for each of the three added terms ($\alpha = 10^{-6}$, $\chi = 100$, and $\gamma = 0.1$) has resulted in reasonable energy estimates for at least three meteorite falls [*Brown et al.*, 2002b, 2004; *Llorca et al.*, 2005], when compared to similar estimates from other data, the seemingly arbitrary (and constant) choice of these parameters is unsatisfying, as certainly the three areas where observations were made have distinctly different surface characteristics. Indeed such values as the air-to-ground coupling efficiency remain uncertain by several orders of magnitude [*Griggs and Press*, 1961; *Hildebrand et al.*,

1997; *Edwards et al.*, 2007] but probably vary according to surface properties [*Edwards et al.*, 2007]. Additionally, it remains unclear whether this relationship, derived from relatively small (~ 2.3 –90 kg) surface explosions, should even apply for the higher-altitude and significantly more energetic meteor sources. Clearly, better scaling relations are needed to infer source energy on the basis of either more realistic modeling or a suite of constrained observations.

[52] Instead of these direct bottom-up approaches, a somewhat more stepwise methodology may be more informative. Understanding the degree of modification (e.g., frequency content, additional phases, and amplitude) the induced seismic wave has from the source airwave and how this relates to the coupling process, over multiple observations, sites, and media, it may be possible to reliably invert observed seismic data to a pseudoacoustic measurement of the airwave. One may then employ existing methods developed in acoustics that are better understood. This approach hinges on the applicability of established theory to explain or reproduce actual observations. Comparative treatments like those of *Kanamori et al.* [1991, 1992] and *D'Auria et al.* [2006] and colocated seismic/infrasonic measurements like those of *ReVelle and Edwards* [2007] and *Edwards et al.* [2007] build confidence in this understanding of the transfer function between atmospheric pressure wave and surface wave.

[53] In a short survey of detections of space shuttle airwaves over California, *Kanamori et al.* [1991, 1992] showed that seismic traces of reentering space shuttle shock fronts recorded on bedrock displayed little in the way of acoustic coupling beyond the initial shock while those stations located in the Los Angeles basin showed significant surface coupling, consistent with simple theory [*Langston*, 2004]. More importantly, they demonstrated for two stations that the synthetic responses of the surfaces computed using the *Ben-Menahem and Singh* [1981, 2000] model (equations (5)–(12)) accurately matched those observed and resulted in reasonable estimates (factor of ~ 2 agreement) of the shock wave overpressure to theoretical calculations at these sites. More recently, *D'Auria et al.* [2006] showed a similar comparative result but explored how the recorded signal could be distorted by the response of short-period sensors. Unfortunately, these studies lacked infrasonic recordings of the corresponding airwave and so comparison to the source function was impossible. Such was not the case for the colocated experiment of *Edwards et al.* [2007]. Here both airwave [*ReVelle and Edwards*, 2007] and surface wave [*Edwards et al.*, 2007] from the Stardust reentry shock wave were recorded simultaneously, and surface elastic properties of the site measured. Using the half-space method (equations (5)–(12)), *Edwards et al.* [2007] simulated the seismic response to within a factor of 2 in amplitude. The results of these separate studies suggests that at least in cases of simple geology or hard bedrock, the half-space method may be sufficient to roughly estimate the source airwave's overpressure. For the more general case, where the surface/near surface is more complex and topography as well as frequency-dependent site response need to be

considered [e.g., Borchardt, 1970; Schlindwein and Koch, 2003; Murphy and Eaton, 2005], inversion for overpressure is unlikely to be this simple. The need for more well-constrained or simultaneous acoustic/seismic measurements of meteor events is clearly necessary to tackle more general cases.

[54] The relations derived for seismoacoustic coupling of meteors on the Earth may prove particularly valuable when seismometers are deployed to Mars [Lognonné et al., 2000]. Despite the Martian atmosphere being significantly less dense at the surface than on Earth (atmospheric conditions are comparable to 30–35 km altitudes on Earth), similar seismoacoustic coupling is predicted by equations (5)–(8) for both rock and unconsolidated soils. Additionally, the rarified Martian atmosphere allows meteoroids to penetrate deeper and should allow the survival of larger meteoroids to impact (and crater) the surface [Christou et al., 2007]. Therefore, it is plausible that Martian seismic monitoring will provide the first estimate of the abundance of meter-sized impactors proximal to the main asteroid belt and the first direct measurements of meteorite impacts on another planet.

8. SUMMARY

[55] The study of seismicity at the Earth's surface created by meteor acoustic/infrasonic sound interactions remains a largely unexplored area of seismology. Driven primarily by the desire to recover freshly fallen meteorites, early work in this area focused upon inversion of observations to constrain trajectories and locations of seismically detected meteors. The results of these early works have shown that for both ballistic and point sources, orientation and position in space can be quite well resolved when adequate coverage of the event is available, while parameters such as velocity and the time of the event's occurrence are more poorly constrained. This uncertainty occurs because of the exceedingly high velocities at which meteoroids typically move through the atmosphere relative to the ambient sound speed, together with the difficulty of adequately approximating the atmospheric propagation field at the time of the event. Thus seismic inversion techniques may only be successful at determining velocities at the low end of typical meteor velocities in ideal cases, while trajectory measurements are much more precise. Fortunately, most meteorite-producing fireballs have velocities below 20 km/s [ReVelle and Wetherill, 1982], leaving open the future prospect of meteorite recovery from seismic data alone.

[56] Although additional constraints, such as signal polarization or visually observed velocities, may be placed upon traveltimes inversions to improve their solutions, the methodology is now well established. At the same time, investigation into what these events may tell us about their source meteoroids and the interaction between the Earth's atmosphere and surface is just beginning. Increasing numbers of seismic networks globally and increased scientific interest means these transient signals are likely to become more commonly reported and available for analysis. Further

calibration among various sites conditions and the acoustic-to-seismic transfer is needed, however, before a “meteor magnitude scale” can be determined.

[57] **ACKNOWLEDGMENTS.** This work was supported by the Natural Sciences and Engineering Research Council. P.G.B. also thanks Natural Resources Canada and the Canada Research Chair Program for additional funding associated for this work.

[58] The Editor responsible for this paper was Michael Manga. He thanks Charles Langston and one other technical reviewer along with one anonymous technical reviewer.

REFERENCES

- Aikman, G. C. L., P. F. Younger, and D. H. Weichert (1989), The daylight fireball of January 20, 1988, *J. R. Astron. Soc. Can.*, *83*, 232–249.
- Aki, K., and P. Richards (2002), *Quantitative Seismology: Theory and Methods*, 2nd ed., Univ. Sci. Books, Sausalito, Calif.
- Anglin, F. M., and R. A. W. Haddon (1987), Meteoroid sonic-wave-generated seismic signals observed at a seismic array, *Nature*, *328*, 607–609, doi:10.1038/328607a0.
- Anglin, F. M., and R. A. W. Haddon (1988), What was that? Meteoroid sonic boom recorded on Yellowknife seismic array, *GEOS*, *17*, 22–25.
- Arrowsmith, S. J., D. P. Drob, M. A. H. Hedlin, and W. N. Edwards (2007), A joint seismic and acoustic study of the Washington State bolide: Observations and modeling, *J. Geophys. Res.*, *112*, D09304, doi:10.1029/2006JD008001.
- Badal, J., U. Dutta, S. Francisco, and N. Biswas (2004), Three-dimensional imaging of shear wave velocity in the uppermost 30m of the soil column in Anchorage, Alaska, *Geophys. J. Int.*, *158*, 983–997, doi:10.1111/j.1365-246X.2004.02327.x.
- Ben-Menahem, A. (1975), Source parameters of the Siberian explosion of June 30, 1908, from analysis and synthesis of seismic signals at four stations, *Phys. Earth Planet. Inter.*, *11*, 1–35, doi:10.1016/0031-9201(75)90072-2.
- Ben-Menahem, A., and S. J. Singh (1981), *Seismic Waves and Sources*, Springer, New York.
- Ben-Menahem, A., and S. J. Singh (2000), *Seismic Waves and Sources*, 2nd ed., Dover, New York.
- Beyer, R. T. (1997), *Non-Linear Acoustics*, Acoust. Soc. of Am., Woodbury, N. Y.
- Biot, M. A. (1956a), Theory of propagation of elastic waves in a fluid-saturated porous solid. I. Low frequency range, *J. Acoust. Soc. Am.*, *28*, 168–178, doi:10.1121/1.1908239.
- Biot, M. A. (1956b), Theory of propagation of elastic waves in a fluid-saturated porous solid. II. Higher frequency range, *J. Acoust. Soc. Am.*, *28*, 179–191, doi:10.1121/1.1908241.
- Bland, P. A., and N. A. Artemieva (2006), The rate of small impacts on Earth, *Meteorit. Planet. Sci.*, *41*, 607–631.
- Borchardt, R. D. (1970), Effects of local geology on ground motion near San Francisco Bay, *Bull. Seismol. Soc. Am.*, *60*, 29–61.
- Borovicka, J., and P. Kalenda (2003), The Moravka meteorite fall: 4. Meteoroid dynamics and fragmentation in the atmosphere, *Meteorit. Planet. Sci.*, *38*, 1023–1043.
- Bronsthen, V. A. (1983), *Physics of Meteoric Phenomena*, D. Reidel, Dordrecht, Netherlands.
- Brown, P. G., A. R. Hildebrand, D. W. E. Green, D. Page, C. Jacobs, D. ReVelle, E. Tagliaferri, J. Wacker, and B. Wetmiller (1996), The fall of the St-Robert meteorite, *Meteorit. Planet. Sci.*, *31*, 502–517.
- Brown, P. G., R. E. Spalding, D. O. ReVelle, E. Tagliaferri, and S. P. Worden (2002a), The flux of small near-Earth objects colliding with the Earth, *Nature*, *420*, 314–316.
- Brown, P. G., D. O. ReVelle, E. Tagliaferri, and A. R. Hildebrand (2002b), An entry model for the Tagish Lake fireball using seis-

- mic, satellite and infrasound records, *Meteorit. Planet. Sci.*, *37*, 661–675.
- Brown, P. G., P. Kalenda, D. O. ReVelle, and J. Borovicka (2003), The Moravka meteorite fall: 2. Interpretation of infrasonic and seismic data, *Meteorit. Planet. Sci.*, *38*, 989–1003.
- Brown, P. G., D. Pack, W. N. Edwards, D. O. ReVelle, B. B. Yoo, R. E. Spalding, and E. Tagliaferri (2004), The orbit, atmospheric dynamics and initial mass of the Park Forest meteorite, *Meteorit. Planet. Sci.*, *39*, 1781–1796.
- Cates, J. E., and B. Sturtevant (2002), Seismic detection of sonic booms, *J. Acoust. Soc. Am.*, *111*, 614–628, doi:10.1121/1.1413754.
- Ceplecha, Z., J. Borovicka, W. G. Elford, D. O. ReVelle, R. L. Hawkes, V. Porubcan, and M. Simek (1998), Meteor phenomena and bodies, *Space Sci. Rev.*, *84*, 327–471, doi:10.1023/A:1005069928850.
- Cevolani, G., L. Foschini, and G. Trivellone (1993), The Lugo fireball of January 19, 1993, *Nuovo Cim.*, *16*, 463–471, doi:10.1007/BF02507654.
- Cevolani, G., M. Hajdukova, L. Foschini, and G. Trivellone (1994), The spectacular airburst over Lugo (Italy) on January 19, 1993, *Contrib. Astron. Obs. Skalnaté Pleso*, *24*, 117–124.
- Chapman, C., W. J. Merline, P. C. Thomas, J. Jonathan, A. F. Cheng, and N. Izenberg (2002), Impact history of Eros: Craters and blocks, *Icarus*, *155*, 104–118, doi:10.1006/icar.2001.6744.
- Christou, A. A., et al. (2007), Comparative studies of meteoroid-planet interaction in the inner solar system, *Planet. Space Sci.*, *55*, 2049–2062.
- Cochran, E. S., and P. M. Shearer (2006), Infrasound events detected with the Southern California Seismic Network, *Geophys. Res. Lett.*, *33*, L19803, doi:10.1029/2006GL026951.
- Collins, G. S., H. J. Melosh, and R. A. Marcus (2005), Earth Impact Effects Program: A Web-based computer program for calculating the regional environmental consequences of a meteoroid impact on Earth, *Meteorit. Planet. Sci.*, *40*, 817–840.
- Cumming, G. L. (1989), Alberta bolide of June 1, 1982: Interpretation of photographic and seismic records, *Can. J. Earth Sci.*, *26*, 1350–1355.
- Dailu, R., and L. Yarong (2007), Seismic analysis for the Lanzhou fireball, *Meteorit. Planet. Sci.*, *42*, 31–35.
- D’Auria, L., E. Marotta, M. Martini, and P. Ricciolino (2006), Seismic and acoustic detection of a bolide airburst in the Gulf of Naples (southern Italy), *J. Geophys. Res.*, *111*, B10307, doi:10.1029/2005JB004254.
- Dorman, J., S. Evans, Y. Nakamura, and G. Latham (1978), On the time-varying properties of the lunar seismic meteoroid population, *Proc. Lunar Planet. Sci. Conf. 9th*, 3615–3626.
- Edwards, W. N., and A. R. Hildebrand (2004), SUPRACENTER: Locating fireball terminal bursts in the atmosphere using seismic arrivals, *Meteorit. Planet. Sci.*, *39*, 1449–1460.
- Edwards, W. N., D. W. Eaton, P. J. McCausland, D. O. ReVelle, and P. G. Brown (2007), Calibrating infrasonic to seismic coupling using the Stardust Sample Return Capsule shockwave: Implications for seismic observations of meteors, *J. Geophys. Res.*, *112*, B10306, doi:10.1029/2006JB004621.
- Ewing, W. M., W. S. Jardetzky, and F. Press (1957), *Elastic Waves in Layered Media*, McGraw-Hill, New York.
- Folinsbee, R. E., J. A. V. Douglas, and J. A. Maxwell (1967), Revelstoke, a new Type I carbonaceous chondrite, *Geochim. Cosmochim. Acta*, *31*, 1625–1635, doi:10.1016/0016-7037(67)90111-1.
- Folinsbee, R. E., L. A. Bayrock, G. L. Cumming, and D. G. W. Smith (1969), Vilna meteorite—Camera, visual, seismic and analytic records, *J. R. Astron. Soc. Can.*, *63*, 61–86.
- Foschini, L. (1998), On the airburst of large meteoroids in the Earth’s atmosphere; The Lugo bolide: Reanalysis of a case study, *Astron. Astrophys.*, *337*, L5–L8.
- Garcés, M. A., and R. A. Hansen (1998), Waveform analysis of seismoacoustic signals radiated during the fall 1996 eruption of Pavlof volcano, Alaska, *Geophys. Res. Lett.*, *25*, 1051–1054, doi:10.1029/98GL00543.
- Griggs, D. T., and F. Press (1961), Probing the Earth with nuclear explosions, *J. Geophys. Res.*, *66*, 237–258, doi:10.1029/JZ066i001p00237.
- Gupta, I. N., and R. A. Hartenberger (1981), Seismic phases and scaling associated with small high-explosive surface shots, *Bull. Seismol. Soc. Am.*, *71*, 1731–1741.
- Halliday, I., and A. T. Blackwell (1971), The search for a large meteorite near Prince George, British Columbia, *Meteoritics*, *6*, 39–47.
- Hildebrand, A. R., P. G. Brown, J. F. Wacker, R. J. Wetmiller, D. Page, D. W. E. Green, C. F. Jacobs, D. O. ReVelle, E. Tagliaferri, and S. A. Kissin (1997), The St-Robert bolide of June 14, 1994, *J. R. Astron. Soc. Can.*, *91*, 261–275.
- Hildebrand, A. R., et al. (1999), The El Paso superbolide of October 9, 1997, *Lunar Planet. Sci.* [CD-ROM], *XXX*, abstract 1525.
- Ishihara, Y., S. Tsukada, S. Sakai, Y. Hiramatsu, and M. Furumoto (2003a), The 1988 Miyako fireball’s trajectory determined from shock wave records of a dense seismic array, *Earth Planets Space*, *55*, E9–E12.
- Ishihara, Y., Y. Hiramatsu, and M. Furumoto (2003b), Ablation process of the 1999 Kobe meteorite inferred from shockwave data, *Eos Trans. AGU*, *84*(46), Fall Meet. Suppl., Abstract P52A-0474.
- Ishihara, Y., M. Furumoto, S. Sakai, and S. Tsukada (2004), The 2003 Kanto large bolide’s trajectory determined from shockwaves recorded by a seismic network and images taken by a video camera, *Geophys. Res. Lett.*, *31*, L14702, doi:10.1029/2004GL020287.
- Jensen, F. B., W. A. Kuperman, M. B. Porter, and H. Schmidt (2000), *Computational Ocean Acoustics*, Springer, New York.
- Johnston, A. C. (1987), Air blast recognition and location using regional seismographic networks, *Bull. Seismol. Soc. Am.*, *77*, 1446–1456.
- Joint Investigation Group on the Kirin Meteorite Shower (1977), A preliminary survey on the Kirin meteorite shower, *Sci. Sin.*, *20*, 502–512.
- Kanamori, H., J. Mori, D. L. Anderson, and T. H. Heaton (1991), Seismic excitation by the space shuttle Columbia, *Nature*, *349*, 781–782, doi:10.1038/349781a0.
- Kanamori, H., J. Mori, B. Sturtevant, D. L. Anderson, and T. H. Heaton (1992), Seismic excitation by space shuttles, *Shock Waves*, *2*, 89–96, doi:10.1007/BF01415896.
- Kanli, A. I., P. Tildy, Z. Pronay, A. Pinar, and L. Hermann (2006), V_s^{30} mapping and soil classification for seismic site effect evaluation in Dinar region, SW Turkey, *Geophys. J. Int.*, *165*, 223–235, doi:10.1111/j.1365-246X.2006.02882.x.
- Klekociuk, A. R., P. G. Brown, D. W. Pack, D. O. ReVelle, W. N. Edwards, R. E. Spalding, E. Tagliaferri, Y. B. Bernard, and J. Zagari (2005), Lidar, satellite and acoustic measurements of an asteroidal airburst in Earth’s atmosphere, *Nature*, *436*, 1132–1135, doi:10.1038/nature03881.
- Langston, C. A. (2004), Seismic ground motions from a bolide shock wave, *J. Geophys. Res.*, *109*, B12309, doi:10.1029/2004JB003167.
- Le Pichon, A., J. M. Guérin, E. Blanc, and D. Reymond (2002), Trail in the atmosphere of the 29 December 2000 meteor as recorded in Tahiti: Characteristics and trajectory reconstitution, *J. Geophys. Res.*, *107*(D23), 4709, doi:10.1029/2001JD001283.
- Lin, T. L., and C. A. Langston (2007), Infrasound from thunder: A natural seismic source, *Geophys. Res. Lett.*, *34*, L14304, doi:10.1029/2007GL030404.
- Llorca, J., et al. (2005), The Villalbeto de la Pena meteorite fall: I. Fireball energy, meteorite recovery, strewn field and petrography, *Meteorit. Planet. Sci.*, *40*, 795–804.
- Lognonné, P., et al. (2000), The NetLander very broad band seismometer, *Planet. Space Sci.*, *48*, 1289–1302, doi:10.1016/S0032-0633(00)00110-0.

- MacCarthy, G. R. (1950), Earth tremors produced by a large fireball, *Earthquake Notes*, 26, 20.
- Malin, M. C., K. S. Edgett, L. V. Posiolova, S. M. McColley, and E. Z. N. Dobrea (2006), Present-day impact cratering rate and contemporary gully activity on Mars, *Science*, 314, 1573–1577, doi:10.1126/science.1135156.
- McDonald, J. A., and T. T. Goforth (1969), Seismic effects of sonic booms, *J. Geophys. Res.*, 74, 2637–2647, doi:10.1029/JB074i010p02637.
- Murphy, C., and D. Eaton (2005), Empirical site response for POLARIS stations in southern Ontario, Canada, *Seismol. Res. Lett.*, 76, 99–109.
- Nagasawa, K. (1978), An analysis of the sonic boom from a great fireball on May 10, 1977, recorded on seismographs of volcano observatories (in Japanese with English abstract), *Bull. Earthquake Res. Inst. Univ. Tokyo*, 53, 271–280.
- Nagasawa, K., and K. Miura (1987), Aerial path determination of a great fireball from sonic boom records on seismographs (in Japanese with English abstract), *Bull. Earthquake Res. Inst. Univ. Tokyo*, 62, 579–588.
- Nicholls, D. C., and I. C. Stewart (1974), The location of meteorite impacts by seismic methods, *Meteoritics*, 9, 223–231.
- Nunziata, C., M. Natale, and G. F. Panza (2004), Seismic characterization of Neapolitan soils, *Pure Appl. Geophys.*, 161, 1285–1300, doi:10.1007/s00024-003-2492-z.
- Oberst, J., and Y. Nakamura (1991), A search for clustering among the meteoroid impacts detected by the Apollo lunar seismic network, *Icarus*, 91, 315–325, doi:10.1016/0019-1035(91)90027-Q.
- Press, F., and M. Ewing (1951), Ground roll coupling to atmospheric compressional waves, *Geophysics*, 16, 416–430, doi:10.1190/1.1437684.
- Pujol, J., P. Rydelek, and T. Bohlen (2005), Determination of the trajectory of a fireball using seismic network data, *Bull. Seismol. Soc. Am.*, 95, 1495–1509, doi:10.1785/0120040155.
- Pujol, J., P. Rydelek, and Y. Ishihara (2006), Analytical and graphical determination of the trajectory of a fireball using seismic data, *Planet. Space Sci.*, 54, 78–86, doi:10.1016/j.pss.2005.08.003.
- Qamar, A. (1995), Space shuttle and meteoroid—Tracking supersonic objects in the atmosphere with seismographs, *Seismol. Res. Lett.*, 66, 6–12.
- ReVelle, D. O. (1974), Acoustics of meteors—Effects of the atmospheric temperature and wind structure on the sounds produced by meteors, Ph.D. dissertation, Univ. of Mich., Ann Arbor.
- ReVelle, D. O. (1976), On meteor generated infrasound, *J. Geophys. Res.*, 81, 1217–1229, doi:10.1029/JA081i007p01217.
- ReVelle, D. O., and W. N. Edwards (2007), Stardust—An artificial, low-velocity “meteor” fall and recovery: 15 January 2006, *Meteorit. Planet. Sci.*, 42, 271–299.
- ReVelle, D. O., and G. W. Wetherill (1982), Relationships between comets, large meteors, and meteorites, in *Comets*, edited by L. L. Wilkening and M. S. Matthews, pp. 297–319, Univ. of Ariz. Press, Tucson.
- ReVelle, D. O., P. G. Brown, and P. Spurny (2004), Entry dynamics and acoustic/infrasound/seismic analysis for the Neuschwanstein meteorite fall, *Meteorit. Planet. Sci.*, 39, 1605–1626.
- Ripepe, M., S. Ciliberto, and M. D. Schiava (2001), Time constraints for modeling source dynamics of volcanic explosions at Stromboli, *J. Geophys. Res.*, 106, 8713–8727, doi:10.1029/2000JB900374.
- Sabatier, J. M., H. E. Bass, and L. N. Bolen (1986), The interaction of airborne sound with the porous ground: The theoretical formulation, *J. Acoust. Soc. Am.*, 79, 1345–1352, doi:10.1121/1.393662.
- Schindwein, V., and K. Koch (2003), A quantitative study of the site effects observed at the GERESS array, *Bull. Seismol. Soc. Am.*, 93, 1051–1064, doi:10.1785/0120020178.
- Shishkin, N. I. (2007), Seismic efficiency of a contact explosion and a high velocity impact, *J. Appl. Mech. Tech. Phys.*, 48, 145–152, doi:10.1007/s10808-007-0019-6.
- Sorrells, G., J. Bonner, and E. T. Herin (2002), Seismic precursors to space shuttle shock fronts, *Pure Appl. Geophys.*, 159, 1153–1181, doi:10.1007/s00024-002-8676-0.
- Stoll, R. D. (1980), Theoretical aspects of sound transmission in sediments, *J. Acoust. Soc. Am.*, 68, 1341–1349, doi:10.1121/1.385101.
- Tatum, J. B. (1999), Fireballs: Interpretation of airblast data, *Meteorit. Planet. Sci.*, 34, 571–585.
- Tatum, J. B., L. C. Parker, and L. L. Stumpf (2000), Sound from a fireball—Distinguishing between the hypersonic shock front and the terminal burst, *Planet. Space Sci.*, 48, 921–923, doi:10.1016/S0032-0633(00)00057-X.
- Urlick, R. J. (1983), *Principles of Underwater Sound*, 3rd ed., McGraw-Hill, New York.
- Wang, R. (1999), A simple orthonormalization method for stable and efficient computation of Green’s functions, *Bull. Seismol. Soc. Am.*, 89, 733–741.
- Whipple, F. J. W. (1930), The great Siberian meteor and the waves, seismic and aerial, which it produced, *Q. J. R. Meteorol. Soc.*, 56, 287–304.
- Whipple, F. J. W. (1934), On phenomena related to the great Siberian meteor, *Q. J. R. Meteorol. Soc.*, 60, 505–513.

P. G. Brown, Department of Physics and Astronomy, University of Western Ontario, 1151 Richmond Street, London, ON N6A 3K7, Canada.

D. W. Eaton, Department of Geoscience, University of Calgary, Calgary, AB T2N 1N4, Canada.

W. N. Edwards, Department of Earth Sciences, University of Western Ontario, 1151 Richmond Street, London, ON N6A 5B7, Canada. (wedwards@uwo.ca)